NASA TECHNICAL NOTE

NASA TN D-8282

NASA TN D-8282

THERMAL PERFORMANCE OF A MODULARIZED REPLACEABLE MULTILAYER INSULATION SYSTEM FOR A CRYOGENIC STAGE

Richard H. Knoll and Richard L. DeWitt

Lewis Research Center
Cleveland, Ohio 44135

NATIONAL AERONAUTICS AND SPACE ADMINISTRATION • WASHINGTON, D. C. • JANUARY 1977

1 Report No	2 Government Accession No	3 Recipient's Catalog No
NASA TN D-8282		

4 Title and Subtitle	5 Report Date
THERMAL PERFORMANCE OF A MODULARIZED REPLACEABLE MULTILAYER INSULATION SYSTEM FOR A CRYOGENIC STAGE	January 1977
	6 Performing Organization Code
7 Author(s)	8 Performing Organization Report No
Richard H. Knoll and Richard L. DeWitt	E-8809
	10 Work Unit No
9 Performing Organization Name and Address	506-21
Lewis Research Center National Aeronautics and Space Administration Cleveland, Ohio 44135	11 Contract or Grant No
	13 Type of Report and Period Covered
12 Sponsoring Agency Name and Address	Technical Note
National Aeronautics and Space Administration Washington, D.C. 20546	14 Sponsoring Agency Code

15 Supplementary Notes

16 Abstract

A rugged modularized MLI system for a 2.23-meter-diameter (87.6-in.-diam) liquid hydrogen tank was designed, fabricated, and tested under simulated near-Earth and deep-space environments. The two blankets of the system were each composed of 17 double-aluminized Mylar radiation shields separated by silk net. The unit area weight of the installed system was 1.54 kg/m^2 (0.32 lb/ft^2). The overall average heat transferred into the insulated tank was 22.7 and 0.98 watts (77.4 and 3.3 Btu/hr) during simulated near-Earth and deep-space testing, respectively. The near-Earth result was only 2.6 times that predicted for an undisturbed insulation system (i.e., no seams or penetrations). Tests indicate that this insulation concept could be useful for a cryogenic Space Tug or orbit transfer vehicle application.

17 Key Words (Suggested by Author(s)) Cryogenic fluid storage, Cryogenic rocket propellants; Liquid hydrogen; Multilayer insulation; Spacecraft thermal protection; Spacecraft thermal testing; Space environment simulation; Thermal insulation

18 Distribution Statement
Unclassified - unlimited
STAR Category 18

19 Security Classif (of this report)	20 Security Classif (of this page)	21 No of Pages	22 Price*
Unclassified	Unclassified	69	$4.50

For sale by the National Technical Information Service Springfield Virginia 22161

Page intentionally left blank

Page intentionally left blank

CONTENTS

THERMAL PERFORMANCE OF A MODULARIZED REPLACEABLE MULTILAYER INSULATION SYSTEM FOR A CRYOGENIC STAGE

by Richard H. Knoll and Richard L. DeWitt

Lewis Research Center

SUMMARY

A rugged, modularized multilayer insulation (MLI) system for a 2.23-meter-diameter (87.6-in.-diam) liquid hydrogen tank was designed, fabricated, and tested under conditions simulating both a near-Earth orbital environment and a deep-space environment. The MLI system consisted of two insulation blankets each made up of alternate layers of double silk net (16 layers) and double-aluminized Mylar radiation shields (15 layers) contained between two cover sheets of Dacron-scrim-reinforced Mylar. The assembled layers of spacers, radiation shields, and cover sheets were held together by nylon button pins and retainers. The insulation system was modularized to facilitate removal and/or replacement of insulation elements. In general, butt joints (with the cover-sheet overlap on each side) or simple overlap joints were used. Nominal layer density of the insulation blankets was 17.7 layers per centimeter (45 layers/in.). The total system weight, including some necessary fairings beneath the insulation blankets, was 23 kilograms (50.8 lb). This corresponds to a unit area weight of 1.54 kg/m^2 (0.32 lb/ft^2).

The average overall heat transferred to the insulated liquid hydrogen tank during simulated near-Earth testing was 22.7 watts (77.4 Btu/hr), of which 19.3 watts (66 Btu/hr) or 1.29 W/m^2 (0.41 Btu/hr ft^2) was chargeable to the insulation. The heat transfer through the insulation as applied was approximately 2.6 times that predicted for a "perfectly" applied system (i.e., no seams or penetrations in the insulation). The overall heat transfer rate into the insulated tank during simulated deep-space testing was 0.98 watt (3.3 Btu/hr) for the lowest vacuum pressure obtained (8×10^{-4} N/m^2 (6×10^{-6} torr)).

Repetitive testing showed some degradation in insulation performance with time. Experimental evidence suggests that the degradation was probably a result of unplanned leakage of gases beneath the insulation rather than a basic degradation in the insulation properties. Overall, the modular insulation system as developed was rugged and easily applied (or replaced) and performed very well considering the simplified seams and attachment methods used. A few repeated tests were run under conditions of cyclic environment (i.e., evacuated tests interspersed by warmups and exposure to atmospheric conditions.) The results of these tests show that this insulation concept may be useful for a cryogenic Space Tug or orbit transfer vehicle application.

INTRODUCTION

Cryogenic propellants are currently used in the Centaur vehicle and have recently been used in the upper stages of the Saturn V launch vehicle. The space flight missions of these upper stages required only short storage times for the cryogenic propellants (7 hr or less) in order to fulfill their mission objectives. For short storage times, foam insulation has been adequate in affording a major portion of the thermal protection for the cryogenic tanks. Extending the in-orbit or deep-space stay times of cryogenic-fueled vehicles will require the use of thermal radiation protection such as multilayer insulation (MLI) and/or shadow shields (e.g., refs. 1 to 3). The D-1T version of Centaur uses both MLI (forward bulkhead) and thermal radiation shielding (3 shields on side wall) on the liquid hydrogen tank to extend its in-orbit stay time (ref. 4). Future development of a cryogenic Space Tug for mission durations of the order of a week will require MLI as opposed to foam insulation (refs. 5 and 6). For some interplanetary missions (e.g., Earth to Saturn), cryogenics may have to be stored for over 3 years and this will also require either MLI or a combination of MLI and shadow shields.

Considerable effort has been spent on MLI technology for basic material or insulation properties (e.g., refs. 7 and 8) and, more recently, in applying the insulation to large-scale tankage (e.g., refs. 8 to 13). In general, most MLI systems are designed for one space flight and as a result have been carefully tailored to a specific propellant tank. For a cryogenic Space Tug or orbit transfer vehicle application, where many successive flights are anticipated, a well-designed reusable system is desired for a multi-use life. Efforts such as those described in reference 13, where a carefully tailored system with reusable elements (e.g., gold-coated Kapton) is used, strive toward this objective. Another approach for the Space Tug application is to design a low-cost, potentially reusable, modularized system that is easily replaced if required. This approach accepts some degradation in performance in exchange for (1) the capability of easily changing the insulation system at <u>any</u> time, either planned or unplanned replacement; (2) the capability of selectively replacing only the damaged portion of the system; (3) lower installation costs; and (4) lower material costs.

This report describes the design, fabrication, and testing of a modularized MLI system developed for a 2.23-meter-diameter (87.6-in.-diam) liquid hydrogen tank. The basic objectives considered in designing the system were (1) to provide an easily applied insulation that was modular in nature and facilitated replacement of all or part of the system and (2) to provide positive density control of the MLI to help ensure repeatable performance. The positive density control is desired to avoid local compression of the inner layers of insulation on the upper portion of the tank and possible deleterious compression during the cyclic pressure fluctuations of repeated ascent and descent of a cryogenic spacecraft such as the Space Tug.

The MLI was one element of a complete integrated thermal protection system (MLI plus shadow shields) designed to demonstrate a capability to store cryogenics (liquid hydrogen and fluorine) for a 1200-day interplanetary mission (ref. 14). All necessary penetrations for structural support, plumbing, and electrical wiring representative of a cryogenic spacecraft were incorporated. Thus, the results closely represent the performance of a flightweight system. The complete test package of reference 14 (incorporating both MLI and shadow shields) was designated the "Cryogenic Storage Test Vehicle" (CSTV). As a part of the work of reference 14, the MLI system was tested under conditions simulating severe near-Earth orbital operations (e.g., inside the cargo bay of the Space Shuttle Orbiter) as well as conditions simulating deep-space operations (e.g., synchronous orbit for an oriented vehicle). For brevity, only those tests pertinent to a cryogenic Space Tug application are reported herein.

Measurements were recorded in U.S. customary units and have been converted to SI units. Both sets of values are given throughout the report.

DESIGN, FABRICATION, AND INSTALLATION OF MULTILAYER INSULATION

Design

Design philosophy. - The purpose of the tank-mounted MLI subsystem for the 1200-day mission was to provide the primary thermal protection for the propellant tanks during ground hold and ascent. Additionally, the MLI supplements the shadow shields, which serve as the primary thermal protection during deep-space operations A sketch of the complete vehicle for the 1200-day mission is shown in figure 1.

Multilayer insulation was decided on for the following reasons: (1) it is as adequate or better than the more conventional foam insulations for the first few hours of the mission and (2) the use of MLI in combination with shadow shields provides a measure of forgiveness if for some reason the shadow shield emittances were to degrade in the space environment. In addition, using MLI provided an opportunity to add to knowledge of MLI applications.

The ground rules used to arrive at a particular design were the following

(1) The system must be rugged in order to minimize any degradation in thermal performance due to handling.

(2) It must be modular so that part or all of the system can be easily removed and replaced.

(3) Substantial baseline performance data must be available in order to evaluate the penalties involved in applying a system.

(4) The performance of the system should be adequate for both reasonable ground-hold and near-Earth heat fluxes (e.g., <631 and 2.21 W/m^2 (<200 and 0.7 Btu/hr ft^2), respectively).

(5) The system should give repeatable performance from test to test.

Basic design. - The basic insulation concept arrived at for the liquid hydrogen tank is shown in figure 2. Two MLI blankets were used. Each blanket contained 15 double-aluminized Mylar radiation shields alternately spaced between 16 double layers of silk-net spacers with two outer structural cover sheets of reinforced double-aluminized Mylar (Schjeldahl X-850). Design data for the materials used are listed in table I. The entire assembly was held together with nylon button pins and retainers (fig. 3), located on 20-centimeter (8-in.) centers These were cemented to the cover sheets at their points of contact to provide a positive means of layer density control for the insulation. In addition, where possible, the cover sheets, spacers, and shields were formed to the contours required to further control the insulation density. Both of these techniques were used to reduce local compression of the insulation caused either (1) by the additional weight pressing on the insulation on the top of the tank (e g., see ref. 15) or (2) by the presence of excess insulation materials resulting from cutting, darting, and overlapping the sheets to fit a double-contoured surface. In this way, deleterious effects of compression (e.g., see ref. 15) could be minimized and the resulting insulation performance should be more consistent and predictable. Nominal insulation layer density based on the button-pin-to-retainer dimension was 17.7 radiation shields per centimeter (45 radiation shields/in.), that is, 15 radiation shields plus two cover sheets per 0.95 cm (0.375 in.).

The double-aluminized Mylar - silk-net combination was used because extensive data were available on its thermal performance (refs. 7, 8, 16, and 17). The reinforced Mylar cover sheets, consisting of a Dacron scrim sandwiched between outer layers of single-aluminized Mylar, were used primarily as structural sheets. Substantial data were also available on the structural properties of this cover sheet material (e.g., ref. 18) since the same material is currently being extensively used on the D-1T Centaur. The button pins and retainers were used in previous MLI technology studies (e.g., ref. 9) but were not cemented to the cover sheets as was done in this study. Velcro hook-pile tapes were used to fasten the inner blanket to the tank. The outer blanket was then attached by the same fastening technique.

For ground-hold thermal protection, the insulation as applied was assumed to provide about 2.5 centimeters (1 in.) of dead helium space for a helium-purged system (e.g., 1.9 cm (3/4 in.) of insulation plus 0.64 cm (1/4 in.) for Velcro attachments). This would result in a calculated, ground-hold design heat flux of approximately 631 W/m^2 (200 Btu/hr ft^2). Higher fluxes for thinner (hence, lighter) insulation systems could have been tolerated, but the level selected was comparable to the flux

experienced by Centaur. Hence, the Centaur experience could be drawn upon with the knowledge that no major ground-hold problem areas would be incurred.

Modular system design. - Figure 4 gives an overall view of the 2.23-meter-diameter (87.6-in.-diam) liquid hydrogen tank. All lines from tank penetrations terminated at an area just below the tank equator (valve box). Modularizing the insulation system in combination with the use of structural cover sheets resulted in an insulation system that was both rugged and easily applied or removed. As shown in figure 5 the insulation comprised several elements, including gore panels, upper polar cap, lower polar cap, fill line, fill line elbow, vent line, valve box, strut penetration, and positioning pin covers.

Details of the gore panel insulation are given in figure 6. The panel consisted of a 60° segment of insulation with a 3° extension of the inner and outer cover sheets on opposing edges to ensure against direct radiation penetration at the seams. This arrangement mitigated the need for careful fitting at the butt joint between adjacent blankets. A continuous Velcro hook tape was cemented to the surfaces of the cover sheet extensions that faced the tank. Mating intermittent Velcro pile tape was cemented to the outward-facing surfaces of the cover sheets and to the liquid hydrogen tank itself. The 1.9-centimeter-wide (3/4-in.-wide) nylon hook tape was applied in a continuous strip (1) because its coefficient of thermal expansion was essentially the same as that of the cover sheet and (2) because it simplified mating with the intermittent pile (avoided alinement problems). The 5.08-centimeter-wide (2-in.-wide) pile tape, which had a coefficient of thermal expansion roughly half that of the cover sheets, was applied in 7.62-centimeter-long (3-in.-long) strips every 33 centimeters (13 in.). Details of the Velcro attachment at the butt joints are also given in figure 6. The offset butt joint between the inner and outer blankets was designed primarily to minimize seam heat leaks.

Offset of the inner and outer blankets (as shown in fig. 6) was achieved by shifting the location of grommets in each blanket by 6°. The grommets (six per panel) slipped over nylon positioning pins that were adhesively bonded to the liquid-hydrogen-tank surface. The positioning pin arrangement on the tank and the relative grommet location in the inner and outer blankets are shown schematically in figure 7. This technique allowed positive location of the gore panels and facilitated quick removel and/or replacement of a panel. Details of the blanket grommets and the tank positioning pins are shown in figure 8.

The insulation for the upper and lower polar caps is shown in figures 9 and 10, respectively. Both insulation caps were in the form of truncated cones and were applied to fiberglass forms, which were in turn attached to the liquid hydrogen tank. The fiberglass forms were required to avoid conforming the insulation around the tank penetrations (i.e., the fill and vent line, etc.) at the top and bottom of the tank. These forms are shown in figure 11.

The upper polar cap insulation (fig. 9) consisted of two separate blankets held together by double-length nylon button pins and retainers. The double-length button pins were 1.9 centimeters (3/4 in.) long and penetrated both blankets. The insulation assembly was in turn held to the fiberglass cover by Velcro hook-pile tape, as shown. The inner blanket had tabs that slipped over the positioning pins and were held in place by a Teflon washer and a stainless-steel retaining pin. The outer blanket covered the positioning pins, extended at least 12.7 centimeters (5 in.) beyond the positioning pins, and was attached to the gore panel insulation with Velcro tape. This type of joint closure is not as efficient thermally as the offset butt joint but makes fabrication and application quite simple and was considered adequate for the application intended. The lower polar cap insulation (fig. 10) was similar in design but had a cutout for the fill line penetration.

Details of the insulation for the fill line, fill line elbow, and vent line were similar. The fill line is shown in figure 12. The insulation consisted of two blankets held together by double-length button pins and retainers. Velcro hook-pile tape was located at discrete points for attachment to the tank or mating insulation panels. An offset butt joint was used for mating with adjacent gore panels and the lower polar cap insulation. The gore panel insulation in the vicinity of the plumbing penetrations is not shown, but it was cut out to mate with the offset butt joints on both the fill line and vent line insulations.

Insulation for the valve box is shown in figure 13. For simplicity the button pins and hook-pile tapes are not shown. They were applied in the same general fashion as for the polar cap insulation. Offset butt joints were used throughout. The insulation was attached to a fiberglass valve box, which was in turn bolted to support brackets welded to the lower hemisphere of the liquid hydrogen tank.

Insulation covers were required for the 12 positioning pins that penetrated the gore panel insulation at the tank equator and for the 12 fiberglass struts that supported the liquid hydrogen tank. These are shown in figures 14(a) and (b), respectively. The positioning pin covers consisted of five layers of double-aluminized Mylar and silk net sandwiched between two reinforced Mylar cover sheets. The edges were sewn, and holes were punched near the periphery to facilitate evacuation of the assembly. Velcro hook tape was cemented to the surface facing the tank for mating with corresponding Velcro pile tape cemented to the gore panels around the positioning pin penetrations. The tank-support-strut penetration cover was made similarly. It also used Velcro tape for attachment to the MLI gore panels but in addition was locally taped to the strut after the extended cover sheet was formed around the strut.

Finally, the approach taken for meteoroid protection was to individually protect any vulnerable area rather than to cocoon the stage in one all-encompassing meteoroid barrier. The protection concept selected was a single layer of beta fiber fabric installed

over the tank insulation blankets. The shield used was made of Teflon-impregnated beta glass cloth and covered the entire tank. Although they are not shown, the meteoroid shield design had gore sectors with polar caps and a valve-box cover similar to the insulation design. It was designed to attach to the insulation with Velcro hook tape mated to the exposed Velcro pile tape on the insulation.

Fabrication

Gore panel insulation. - The gore panel insulation fabrication is reported in detail in reference 19; however, a brief description is given here. As indicated previously it was desired to form the insulation components (i.e., shields, spacers, and cover sheets) to the tank contour to help control the insulation layer density. Several methods of forming the shields completely to contour were tried, but most resulted in severe degradation of the shields' emissivity in the areas of the shield that were subject to high stretch. A compromise method used to reduce the emissivity degradation to achieve an average emissivity of approximately 0.05 involved draping the insulation pack in a forming tool and only partially forming the material. Figure 15 shows the forming of the aluminized Mylar radiation shields 17 at a time in a pack. The result of this forming is shown in figure 16 for a typical radiation shield. The silk-net spacers were formed by soaking in water, laying and smoothing out to the desired contour, and air drying, as shown in figure 17. The reinforced Mylar cover sheets were formed by first thermal vacuum forming to the approximate shape and then hand ironing to the desired contour. Only partial forming by the thermal vacuum process was possible because of the springback of the Dacron threads within the reinforced Mylar. Hand ironing of partially formed cover sheets, shown in figure 18, involved locally shrinking the bunched areas of the sheet.

The preformed radiation shields and silk-net spacers were rough trimmed and then assembled on the layup tool shown in figure 19(a). Tape was used to temporarily hold the radiation shields in place. The outer structural cover sheet was not applied until the blanket edge, which would be hidden by the cover sheet overlap, was trimmed. After the one edge of the blanket was trimmed, the trim template was removed and the rough-trimmed outer cover sheet was applied. The trim template was then reapplied as shown in figure 19(b), and several button pins and retainers were inserted to stabilize the assembly. Final trim of the blanket was then made with a metal shim protecting the inner cover overlap of the other edge of the blanket. The grommet holes were cut with a hollow punch.

After final trimming, the trim template was removed and the remaining button pins, retainers, and grommets were applied. The button pins were applied by placing a

hollow needle over the stem of the button pin and then penetrating the blanket from underneath at the hole locations in the layup tool (fig. 19(a)). The contact face of the button pin was coated with a polysulfone adhesive (Pro-Seal 501) prior to penetrating the blanket. The hollow needle was then removed, and a retainer with adhesive was snapped in place on the button pin shaft. The shaft extension was then melted with a hot iron to form a ball. This particular button application technique was used for all elements of the insulation system. The contact surfaces of the grommets were also coated with an adhesive before they were applied to the blanket

After a 24-hour, room-temperature air cure of the adhesive, the Velcro hook-pile tapes were similarly cemented to the blanket in the desired pattern with Pro-Seal 501 polysulfone adhesive.

Polar cap insulation. - Fabrication of the upper and lower cap insulation required layup forms with holes for installing the button pins much the same as the fabrication of the gore panels. Because the insulation was in the form of a truncated cone, developments of these surfaces were formed from flat sheets for the layup tools and the cover sheets, shields, and spacers.

Figure 20(a) shows the upper polar cap insulation near its final stage of completion. Both the inner and outer blankets are in position for application of the double-length nylon button pins and retainers that will secure the two blankets to each other. The two blankets are also about to be joined at the truncated portion of the cone. This was accomplished by cementing the extended cover sheet tabs from the inner and outer blankets between two annular rings of cover sheet material. The tabs shown on the lower edge of the inner blanket are for attachment to the positioning pins on the upper portion of the tank (fig. 9). Other means of attachment to the upper fiberglass form and tank insulation are by Velcro tape, which has yet to be added. The cover sheets for the outer blanket were joined with aluminized Mylar tape at the lower edge of the insulation blanket. Because the tape tended to seal the system, vent holes were made in the inner cover sheet as shown in figure 20(a).

The completed insulation for the lower polar cap (less the double-length button pins and retainers) is shown in figure 20(b). Fabrication was similar to that for the upper polar cap except for the truncated portion of the cone. Here the insulation was carried over the truncated portion. This was accomplished by cutting and darting the insulation and locally folding and taping each individual shield and spacer. The folder taps of each of the four cover sheets were then cemented to annular rings of cover sheet material, as was done on the upper polar cap. The cutout in the insulation was designed to mate with the fill line elbow insulation by forming an offset butt joint. The extension of the cover sheet over the external butt joint was achieved by taping a strip of cover sheet material along the edge of the blanket with double-stick Mylar tape.

Fill line, fill line elbow, and vent line insulation. - Because of the double-curved surfaces, fabrication of the fill line, fill line elbow, and vent line insulation involved custom forming the various component materials. The cover sheets were cut and attached with aluminized Mylar tape to the desired contour. The silk net was water formed and the aluminized Mylar radiation shields were cut, darted, and locally taped. Tools with the desired contour for the insulation sections were formed from fiberglass. The tools also contained holes for application of the button pins. Figures 21(a) and (b) show the fill line insulation and fill line elbow insulation, respectively. Figure 21(a) shows both the inner and outer blankets for the fill line. The blankets were subsequently joined with double-length button pins and retainers to complete the assembly. Figure 21(b) shows the fill line elbow insulation mated to the lower polar cap insulation. When installed on the tank the elbow insulation overlapped the mating fill line insulation.

The vent line insulation was fabricated like the fill line insulation.

Valve-box insulation. - The valve-box side insulation was fabricated by (1) preassembling the blankets with clips in a flat strip long enough to encircle the valve box, (2) by wrapping the box with the blankets and allowing slippage at the four corners, (3) by adding several button pins and retainers to secure the blankets, and (4) by trimming the blankets to the desired dimensions on the fiberglass valve-box side. Once the trimming was complete, the remaining button pins and retainers were added, along with the Velcro tape, for attachment to the tank and/or the adjacent blanket. Holes were located in the valve-box side for application of the button pins.

The valve-box lid insulation was assembled layer by layer on the fiberglass lid and consequently required formed sheets. The silk-net spacers were water formed, but the cover sheets and radiation shields were cut and taped to the desired contour. The fiberglass lid was used as the layup tool and contained holes for button pin application.

Positioning pin and strut covers. - The 15.2-centimeter-diameter (6-in.-diam) positioning pin covers required a slight curvature to help clear the positioning pins at the tank equator. An aluminum tool with the desired curvature was used to water form the silk net and to heat form the cover sheets. Springback of the cover sheet during heat forming was insignificant for this application. After forming, the insulation was assembled and held temporarily with clips while the perimeter was sewn with Dacron thread. After sewing, the covers were trimmed and Velcro hook tape was added for subsequent attachment to mating Velcro pile tape around the grommets on the gore panels. Holes were punched near the perimeter to ensure low internal pressures during vacuum testing.

The covers for the struts were similarly assembled except that no attempt was made to apply a curvature since in their application the covers had to be severely deformed to partially encircle the strut.

Meteoroid shield. - The shield material was Teflon-impregnated beta glass cloth. The meteoroid shield consisted of gore panels, polar caps, line covers, and a valve-box cover. All elements were fabricated from flat sheets. The 60° gore sectors were fabricated from three 20° developed segments sewn together with Dacron thread. Adjacent sections of the meteoroid shield were attached to the insulation surface by means of mating Velcro hook-pile tape sewn to each surface. In addition, a running stitch using Dacron thread was applied between (1) the gore sectors and the edges of the polar caps, (2) the gore sectors and the line covers, and (3) the line covers and the valve-box cover.

Installation

The first step in installing the insulation system was the adhesive bonding of the positioning pins and the Velcro pile tape to the tank, as shown in figure 22. The adhesive used for both the pins and tape was a thermoplastic polyester resin system (Plyobond 4001 with Plyobond 4004 curing agent). Light pressure was applied during curing. The positioning pins required a 5.7-centimeter-diameter ($2\frac{1}{4}$-in.-diam) overlay of fine-mesh fiberglass cloth applied over the pin base to adequately secure the pin (barely visible on equator pins in fig. 22). Tests of the pins demonstrated that loads as high as 0.91 kilogram (2 lb) could be cantilevered off the pin end at liquid hydrogen temperatures with no failures. The load tests were performed because the positioning pins also share some of the insulation weight with the Velcro pads.

Next the gore panel insulation was applied. Figure 23 demonstrates several stages of the insulation application. The initial step involved trimming the gore panels that straddled the valve-box area so that they could be mated with the insulation covers on the fill line, vent line, and valve box (fig. 23(a)). The trimming was done on a fiberglass mockup of an 180° segment of the tank. After the modified gores were applied to the right of the valve-box area, the remaining inner and outer gore panels were slipped into position, proceeding to the right around the tank. Figure 23(b) shows the panels applied over 75 percent of the tank surface. The detail of the offset butt joint with the cover sheet extensions is evident. The plastic stripping shown was applied over all the Velcro pile tape during panel application to avoid premature closure of the Velcro while the panels were being slipped into a place over the positioning pins.

Once a panel was properly positioned the stripping was pulled out and pressure was applied over the Velcro areas to ensure their closure. Figure 23(c) shows the detail at the tank support area, where the inner and outer blankets had to be cut to facilitate

blanket removal once the tank supports were connected. Also shown is the detail around the positioning pins. The pin is shown with its Teflon washer and stainless-steel retaining pin applied. The Velcro around the pin area is for attachment of the positioning pin covers.

After all gore sectors were in place, the vent and fill line insulations were applied. Figure 23(d) shows the vent line insulation in detail. The offset butt joint for the vent line insulation is evident, as well as the stepped joint for the valve-box insulation. Figure 23(e) shows the system with the valve-box side insulation and positioning pin covers added.

At this point the tank was mounted within its structure for insulation completion. Figure 24 demonstrates the steps involved in applying the upper polar cap insulation. The meteoroid-shield gore panels were applied prior to adding the polar caps because support straps for the shields have to be attached to the upper and lower positioning pins. These straps are evident in figure 24(a). The first step involved attaching the fiberglass form over the upper tank penetrations (i.e., vent line, electrical feedthroughs, etc). Then plastic strips were placed over the Velcro, and the cap insulation was applied (fig. 24(b)). The plastic strips were then removed and the closure made on the Velcro tape. Finally (for the upper polar cap only), an insulation disk was attached to the truncated portion of the fiberglass cap as shown in figure 24(c). Application of the polar cap meteoroid shield then followed. Although not shown, the lower polar cap insulation was applied in the same general manner.

The completed system is shown in figure 25. Details of the tank supports and the complete test package are given in subsequent sections. The total weight of the installed insulation system was approximately 23 kilograms (50.8 lb), including 3.9 kilograms (8.6 lb) for the fiberglass caps and valve box. Considering the surface area of the propellant tank, this weight transfers into a unit area value of 1.54 kg/m^2 (0.32 lb/ft^2).

TEST PACKAGE AND TEMPERATURE CONDITIONING SHROUD

In addition to the tank-mounted insulation system the other major subdivisions of the test package were the liquid hydrogen tank itself, 12 fiberglass support struts, two sections of vehicle structure, a payload simulator, and a constant-temperature equipment box (figs. 1 and 25). During the test series the package was contained within a temperature-controllable shroud and, further, all flow-line and wiring connections were thermally isolated from the facility.

Test Tank

The liquid hydrogen tank (figs. 4 and 22) was an approximate 1.2:1.0 oblate spheroid of 4.96-cubic-meter (175.0-ft^3) actual volume with major and minor diameters of 2.23 and 1.85 meters (87.6 and 73.0 in.), respectively. The tank was constructed of 2219-T62 aluminum and had a working pressure of 55 N/cm^2 differential (80 psid). Both the upper and lower shells of the tank were chemically milled to a membrane thickness of between 0.196 and 0.221 centimeter (0.077 and 0.87 in.). Weld lands were 0.457 centimeter (0.180 in.) thick. Support loads were introduced into the tank by support brackets welded to the tank lower shell. Vent, pressurization, and liquid hydrogen fill and outflow valves were mounted on channel-shaped brackets also welded directly to the lower half of the tank. A burst disk assembly was also included for safety reasons.

Fiberglass Struts

The 12 liquid-hydrogen-tank support struts consisted of filament-wound fiberglass tubes with integral titanium end fittings. The titanium end fittings had a threaded hole to accommodate spherical rod-end bearings that served as the connection device to the tank brackets and the vehicle structure. The struts were 3.8 centimeters (1.5 in.) in diameter and had a minimum wall thickness of 0.076 centimeter (0.030 in.). A mixture of chopped aluminized Mylar and Dexiglas flakes was inserted into the strut tubes to inhibit radiation heat transfer inside the hollow strut. A typical strut is shown as figure 26. Details of the structural design, the thermal design and analysis, and the developmental testing of these struts are available in reference 20.

Vehicle Structure

The structure was a stainless-steel, open-truss type and had two major components designated as (1) the forward structure and (2) the midstructure. These sections can be seen in figure 25.

The forward structure consisted of a circular payload support ring connected to 12 struts that were joined at six equally spaced points on the ring. The midstructure consisted of a hexagonal frame (midstructure support ring) that supported the fuel tank at six node points. Twelve midstructure struts also joined at these six points.

Payload Simulator and Constant-Temperature Equipment Box

The vehicle payload was only simulated thermally and contained no vehicle flow subsystems or electronics superfluous to the immediate testing. The payload simulator was a 3.0-meter-diameter (10-ft-diam), 0.64-centimeter-thick (1/4-in.-thick) aluminum plate bolted directly to the forward-structure payload ring. The bottom surface of the simulator, the side facing the propellant tank, had a measured emittance of 0.076 at room temperature. Onto the back (or top side) of the simulator, 2.5-centimeter-inside-diameter (1-in.-i.d.), D-shaped, liquid hydrogen flow tubes were welded to enable cooling of the simulator to 22 K (40° R). In addition, electrical resistance heater strips were adhesively bonded between the liquid hydrogen flow tubes to allow heating of the simulator to room temperature.

Gaseous helium was chosen as the pneumatic valve operator fluid and propellant tank pressurant for this test package. All helium flow control equipment was housed in a small insulated box, referred to as the equipment box, of approximately 0.08-cubic-meter (2.83-ft^3) volume that was mounted on top of the payload simulator. Pressure switches built into the tank pressurization system were mounted on an unheated plate (referred to in fig. 25 as the pressure switch plate) that was tied to two of the struts of the midstructure. These units were not used during the thermal evaluation testing discussed in this report and hence will not be discussed further.

Shroud

During part of the test program a requirement existed that the test package see a surrounding environmental temperature of approximately 22 K (40° R) In addition, during the other part of the testing, the surrounding environmental temperature had to be maintained at approximately 294 K (530° R). As a result, the vehicle was encased in a cylindrical shroud nominally 3.9 meter (13 ft) in diameter and 3.9 meter (13 ft) high. Figure 27 shows the shroud positioned in the vacuum chamber. The cylindrical body of the shroud was composed of 12 flat panels with vertical, D-shaped, liquid hydrogen flow tubes of 2.5-centimeter (1-in.) inside diameter welded onto the outside surfaces. Both the bottom and top of the shroud were flat and also had liquid hydrogen flow tubes mounted on their exterior surfaces. The fourth major part of the shroud assembly was an annular baffle. This unit, which was also capable of being cooled with liquid hydrogen, was mounted inside the shroud and coplanar with the payload simulator. Its purpose during testing was to minimize radiative heat transfer reflections from the shroud top and the wall above the baffle down to the insulated liquid hydrogen tank. The basic construction of all shroud surfaces was 0.32-centimeter-thick (1/8-in -thick) aluminum

plate. To improve the absorptivity of the shroud, the inside surfaces of the cylindrical body, the bottom, and the top, as well as the top surface of the baffle, had a covering of 0.95-centimeter (3/8-in.) hexagonal honeycomb that was 0.95 centimeter (3/8 in.) thick. These honeycomb surfaces were sprayed with 3M Black Velvet paint. On each major section of the shroud (i.e., vertical walls, bottom, top, and baffle), resistance heaters were adhesively bonded between the liquid hydrogen flow tubes to allow heating of the surfaces to room temperature.

Each section of the shroud was connected to a pressurized circular ring manifold located at the base of the vertical walls. However, each part had an independent vent line containing a two-position flow control valve. During low-temperature operation the control circuits of these valves were regulated by the output of platinum resistance temperature sensors located in the hydrogen lines between the valves and the surfaces being cooled. To reduce radiant heat transfer from the chamber to the shroud, and ultimately the amount of liquid hydrogen used during cryogenic operations, a single layer of double-aluminized Mylar was draped around all exterior surfaces of the shroud. This is shown in figure 28.

THERMAL ISOLATION OF TEST TANK

All the plumbing and electrical wiring required for the test vehicle can be divided into two distinct groups. The first group consists of those flow lines and electrical wires needed as part of the vehicle itself. These lines and wires ran from the payload simulator to the liquid-hydrogen-tank valve box through the pressure switch plate. Any heat transferred along these lines and wires was attributed to the way the vehicle was designed and was considered as part of the expected flight heat loading of the propellant tank.

The second group of lines and wires consisted of those needed for tank flow operations, test instrumentation, and control purposes This group would not be necessary on a flight vehicle but were, however, needed for testing operations and data collection. The test vehicle was designed so that the operations flow lines, the instrument wires from temperature transducers in the tank and insulation, and the control wires from shutoff valves were all brought out at the same location on the tank. After leaving the tank this second group of lines and wires passed through an enclosed duct to a second liquid hydrogen tank, called a cold guard tank, located immediately outside the wall of the shroud. This tank was 0.46 meter (1.5 ft) in diameter and 1.4 meter (4.6 ft) high. It was kept filled with liquid hydrogen during all thermal testing of the vehicle. All plumbing lines passed directly through this tank and, as a result, were completely submerged in liquid hydrogen for at least 1.2 meters (4 ft) of their length. Temperature

conditioning of the instrumentation and control wires was obtained by adhesively bonding them onto the outside of the cold guard tank for a length of approximately 1.5 meters (5 ft).

The insulated, liquid hydrogen, cold guard tank mounted on the MLI-protected shroud can be seen in figure 28.

TEST FACILITY

All thermal testing of the vehicle was done in a 7.6-meter-diameter (25-ft-diam), spherical, side-loading vacuum chamber (figs. 27 and 28). The entrance door to the chamber had a diameter of 6.1 meters (20 ft). The "clean-dry-empty" vacuum capability was approximately 1.1×10^{-4} N/m^2 (8×10^{-7} torr).

Figure 29 is a general schematic of facility plumbing and control circuits required for this experimental program. Liquid hydrogen had to be furnished to the insulated test tank, the cold guard tank, the shroud, and the payload simulator. Hydrogen flow through the simulator was controlled in the same manner as for the shroud. Parallel flow paths in the vent lines of both the test tank and the cold guard tank allowed independent filling of these tanks.

Electric power and heater control circuits were needed for the shroud, the payload simulator, and the equipment bay. The shroud had four separate heater circuits (on the side walls, bottom, top, and baffle); the payload simulator had three separately controlled areas (a center circle and two annular rings); the equipment box was on a separate single circuit.

Several test periods were required at pressure levels higher than the chamber minimum vacuum. These vacuum levels were created by adjusting a controlled bleed of gaseous helium into the chamber outside the shroud enclosure.

A major piece of equipment in the vent lines of both the test and cold guard tanks was the backpressure control valve and its associated control equipment. Figure 30 is a block diagram of the two parallel backpressure control circuits used during this test program. The particular pressure transducers employed were a high-resolution capacitance type. These units sensed any pressure differential between the tank they were monitoring and a "constant" pressure held in a reference bottle located in an ice bath outside the environmental chamber. The output of each differential pressure transducer was used as an input signal to the controller of a valve in the vent line of each tank. More detail on this system can be obtained from references 14 and 21.

INSTRUMENTATION

One of the objectives of the instrumentation was to provide sufficient temperature data so all heat transfer rates and energy content changes of the insulation, tank, ullage, and liquid propellant could be determined. Another objective was to determine the mass flow rate and energy content of the vent gases. In addition, steady-state temperature data for the vehicle structure and the tank-mounted insulation system were also needed (1) to allow verification of the analytical program that was used to predict thermal performance of the test hardware and (2) to determine the effectiveness of construction techniques used in the insulation fabrication.

Thermocouples and platinum resistance temperature sensors (PRTS) comprised the temperature transducers on the test configuration. The majority of the temperature transducers employed were Chromel-constantan thermocouples. Figure 31 is a schematic of the instrumentation on the test package.

The use of PRTS on the test vehicle was confined to the tank interior, the tank wall, several locations on the fiberglass struts, two places on the midstructure, three places within the insulation blankets, and on the payload simulator. The leads from the PRTS, except for the six transducers that were mounted on and thermally shorted to the payload, all exited from the test configuration through the duct from the liquid hydrogen tank to the cold guard tank. The majority of the PRTS used were spanned from 20 to 39 K (36° to 70° R). The probable error of the complete measurement channel was computed to be ±0.2 K at 20 K (±0.36° R at 36° R), which improved to ±0.13 K at 39 K (±0.23° R at 70° R). For PRTS used to measure temperatures on the structure, the insulation blankets, the pressure switch plate, and the payload simulator, the probable error was ≤±1.6 K (≤±2.9° R).

All thermocouples on or within the insulation, on tubes beneath the insulation, and on the tank fiberglass struts were 0.25-millimeter-diameter (10-mil-diam) Chromel-constantan and were referenced to 78 K (140° R) electronic ovens. The thermocouples on the structure were also of 0.25-millimeter-diameter (10-mil-diam) Chromel-constantan; however, they exited from the test hardware through connectors mounted on the payload simulator. They were also referenced to 78 K (140° R) electronic ovens. Each Chromel-constantan thermocouple measurement channel had a computed probable error of ±2.7 K at 20 K (±4.8° R at 36° R), which improved to ±0.79 K at 100 K (±1.4° R at 180° R) and then dropped off to ±2.7 K at 294 K (±4.8° R at 530° R). The equipment box temperature was monitored by four 0.25-millimeter-diameter (10-mil-diam) copper-constantan thermocouples referenced to an ice-point electronic oven. The instrumentation channels for these transducers had a probable error of ±0.44 K at 294 K (±0.8° R at 530° R).

All temperature sensors located on the insulation cover sheets were mounted by

first laying a strip of double-backed Mylar tape (2.5 cm (1 in.) wide) along the isothermal path desired for the wires. For the tank-mounted insulation system this path was at least 30^{o} of the tank meridional distance at the level of the transducer measurement point. The transducer and its lead wires were then laid on the exposed tape surface, and the assembly was covered with aluminized Mylar tape.

Temperature sensors on cylindrical surfaces (e.g., tank fiberglass support struts, vehicle structure struts, and the inside surface of the duct from the liquid hydrogen tank to the cold guard tank) had their lead wires laid on an isotherm for 180^{o} and then were adhesively bonded from the transducer to the point where the wires left the cylindrical surface.

Temperature sensors located on surfaces having little or no curvature (e.g., tank wall, cold guard tank, payload simulator) and their lead wires were also mounted and temperature conditioned by adhesively bonding them along an isotherm

Liquid-level sensors and PRTS inside the test tank were mounted on a low-mass, Bakelite support rake hung from the test-tank lid. In addition, a resistor was also mounted on this rake to allow dissipation of electrical energy into the liquid propellant.

Temperatures of the individual shroud surfaces (e.g., top, each baffle, vertical sides, and bottom) were also measured. A total of 13 PRTS and 9 Chromel-constantan thermocouples were used. All transducers and sections of their lead wires were attached by adhesive bonding.

Hot-cathode tubulated (enclosed) ionization gages were used to measure the vacuum level at two positions inside the shroud volume and at one position in the chamber outside the shroud. The transducers inside the shroud were mounted approximately 0.3 meter (1 ft) off the shroud floor and faced the vertical centerline of the shroud. The chamber gage was mounted at the middle of the chamber "side wall" and faced inward toward the shroud. A copper-constantan thermocouple was bonded on the tubulation of each gage to measure its operating temperature.

Five mass flowmeters were used to measure the test-tank boiloff gas flow rate. Their ranges were 0 to 49.8, 0 to 2.83, 0 to 0.28, 0 to 0.03, and 0 to 0.003 m^3/hr (0 to 1760, 0 to 100, 0 to 10, 0 to 1, and 0 to 0.1 $stdft^3/hr$). These units were remotely valved into the test-tank vent line as the boiloff rate came within their respective ranges. For any given boiloff rate the smallest range meter applicable was always employed. A standard copper-constantan thermocouple and a bonded strain-gage pressure sensor were used directly upstream of the bank of meters. The probable error for each of these mass flow measurement channels was ±2.5 percent of full scale of the transducer range.

Measurements were recorded on an automatic voltage digitizing system and/or continuous, direct-reading, strip charts. Digitized data were recorded only periodically,

the frequency depending on whether the test hardware was going through a transient or a steady-state condition.

TEST CONDITIONS AND PROCEDURE

The test vehicle structure and insulation system were exposed to the three different temperature environments demonstrated in figure 32. The first condition, descriptively referred to as Near Earth, required that the vehicle payload and the shroud be maintained at approximately 294 K (530° R). The Null test condition required that both the payload simulator and the shroud be cooled with liquid hydrogen. During Deep Space, the third test condition, the payload was warmed and maintained at 294 K (530° R) while the shroud remained at liquid hydrogen temperature. Variations of these test conditions were steady-state periods at pressure levels higher than the chamber minimum vacuum. The cold guard tank was filled with liquid hydrogen during all test conditions.

The test procedure started with evacuating the chamber and then cooling the warm test tank and insulation system by filling the tank against a controlled backpressure of at least 13 N/cm^2 abs (19 psia). The decreasing boiloff flow rate was only roughly monitored by splitting the flow between the group of boiloff meters and the tank main vent line. Intermittent topping of the tank was continued during an additional insulation cooling period after the fill. Once the boiloff was below approximately 49.8 m^3/hr (1760 $stdft^3/hr$), the topping process was discontinued and the tank fill backpressure control valve (fig. 29) was closed. The tank was then slowly vented (using the run backpressure control valve) to the desired steady-state pressure. The run backpressure control system was then put into automatic operation. Filling of the cold guard tank was accomplished in like manner by using its fill and run backpressure control valves. The pressure in the cold guard tank was always maintained above the pressure in the insulated test tank during all fill, steady-state, and retopping operations. During steady-state testing the differential between the tanks was maintained constant at either 200 or 930 N/m^2 (1.5 or 7 mm of mercury).

Pressure levels other than the chamber minimum vacuum were created by bleeding ambient-temperature gaseous helium into the chamber. Flow was manually controlled by a micrometer needle valve located immediately outside the chamber wall.

During all the test work conducted, periodic mass spectrometer checks indicated that a helium background existed in the chamber and shroud volume. In addition, when the shroud was being operated at liquid hydrogen temperature, the tubulations of the ion gages inside the shroud volume were considerably colder than during Near-Earth conditions. As a result, both a helium gas correction and a gage operating temperature correction were made on the shroud volume vacuum level readings taken during the Null

and Deep-Space test periods. The correction applied for the helium background was obtained from reference 22. The correction applied because of different gage tubulation temperatures is detailed in appendix C of reference 14.

DATA REDUCTION

The basic procedure used for data reduction was to subtract all solid-conduction heat flows, as well as energy-content changes of the insulation, tank, ullage, and liquid propellant, from the heat equivalent of the gross boiloff value of the insulated tank. The net boiloff value obtained gave the heat flow through the insulation blankets as follows:

$$\underbrace{QBLKTS}_{\substack{\text{Heat transferred through uninterrupted insulation blankets}}} = \underbrace{QBOILOFF}_{\substack{\text{Latent and sensible heat content of boiloff gas}}} \underbrace{- DULLAGE - DTANK - DINSUL - DLIQUID}_{\substack{\text{Energy content increase of ullage volume, tank wall, insulation system, and liquid propellant}}}$$

$$- \underbrace{QSTRUTS}_{\substack{\text{Heat added by conduction down fiberglass struts}}} - \underbrace{QDUCT}_{\substack{\text{Heat added to tank by conduction through valve-box wall and by radiation from duct volume}}} - \underbrace{QWIRES}_{\substack{\text{Heat added by conduction through instrumentation and control wires}}} - \underbrace{QPLUMBING}_{\substack{\text{Heat added by solid conduction through service lines and tubes connected to test tank}}}$$

$$- \underbrace{QPINS}_{\substack{\text{Heat added by solid conduction through nylon positioning pins}}} - \underbrace{QPEN.\ EFFECTS}_{\substack{\text{Increased heat transfer through blankets due to penetration of fiberglass struts}}} - \underbrace{QSEAM}_{\substack{\text{Increased heat transfer through blankets due to presence of seams in blankets}}} \quad (1)$$

(See appendix for definition of all symbols.) Every term on the right side of the equation was either experimentally evaluated during this program or derived as a direct result of work reported in reference 23. The term QBLKTS was then obtained directly by subtraction.

The term QBOILOFF is defined as the total latent and sensible heat gained by the liquid propellant evaporated during the boiloff process. After leaving the test tank and passing the backpressure control valve the gas was measured by a mass flowmeter. Temperature and static pressure transducers located immediately upstream of the flowmeter verified that the statepoint of the gas was within the operating limits of the meter. The mass flow rate of gas was determined by using the equation

$$\dot{M}_{bo} = \dot{V}_{bo}\rho_{stp} \tag{2}$$

where $\rho_{stp} = \rho(294\ \text{K}\ (530^{\circ}\ \text{R});\ 1\times10^{5}\ \text{N/m}^2\ (760\ \text{mm of mercury})$. The mass flow rate was monitored constantly by a strip-chart recorder during the entire test period. Discrete data points were recorded on magnetic tape at least every 20 minutes during the steady-state periods. The value of QBOILOFF was then calculated from the magnetic tape data by the equation

$$\text{QBOILOFF} = \underbrace{\dot{M}_{bo}\lambda\left(\frac{\rho_{liq}}{\rho_{liq} - \rho_{sv}}\right)}_{\text{Latent heat}} + \underbrace{\dot{M}_{bo}(h_{tv} - h_{sv})}_{\text{Sensible heat}} \tag{3}$$

The factor $\rho_{liq}/(\rho_{liq} - \rho_{sv})$ corrects for the vapor that was formed but did not leave the test tank; it merely occupied the space vacated by the evaporated liquid.

Since the tank and the environmental chamber pressures, as well as the shroud and payload temperatures, were maintained constant during each steady-state period, it was expected that there would be no change in the energy content of the ullage, the tank wall, the insulation, or the liquid hydrogen propellant. However, to detect any changes that might occur, temperature sensors were employed throughout these volumes and materials. Each sensor was assigned a volume of material, and any change in that temperature would result in an energy-content change.

For the first three energy changes (i.e., DULLAGE, DTANK, and DINSUL) a close examination was made over all steady-state periods of the temperature values required for their calculation. This study revealed that the experimentally measured temperatures used in the calculation of each energy change varied by less than its expected margin of error. The conclusion reached, therefore, was that these energy changes were

below our level of detection and, hence, were considered to be zero for all steady-state periods reported herein.

While the accuracy of the platinum resistance temperature sensors used in calculating DLIQUID was ±0.2 K at 20 K (±0.36° R at 36° R), we found that saturation temperature changed by less than $\pm 0.78 \times 10^{-5}$ K ($\pm 0.14 \times 10^{-4}$° R) during any steady-state period. This value resulted from a review made of the tank pressure history during all steady-state periods. No pressure changes equal to or greater than ±0.27 N/m^2 (±0.002 mm of mercury), the limit of strip-chart resolution, were found to have occurred. The temperature variation of $\pm 0.78 \times 10^{-5}$ K ($\pm 0.14 \times 10^{-4}$° R) corresponds to a DLIQUID change of only ±0.0059 watt (±0.02 Btu/hr). Since this is a small value, DLIQUID was assumed to be zero for all steady-state periods.

The terms QSTRUT, QWIRES, QPLUMBING, and QPINS were composed of pure conduction and were evaluated by using the Fourier heat transfer equation

$$Q_{cond} = \frac{A}{L} \int_{T_1}^{T_2} k(T)\,dT \tag{4}$$

The term QDUCT had both a conduction and a radiation component. The conduction term was evaluated by using equation (4); the radiation term was obtained from the equation

$$Q_{rad} = \sigma A T^4 \tag{5}$$

The area A was that of the box-to-duct opening, and the temperature T was determined from a thermocouple located on the duct. The duct was considered to be a perfect emitter, and the interior of the tank valve box was considered to be a perfect absorber.

The technique for determining values for the seam effect (QSEAM), as well as for the effect of the fiberglass strut penetrations (QPEN. EFFECTS), is given in the RESULTS AND DISCUSSION section.

RESULTS AND DISCUSSION

Overall Test Sequence

For clarity, the test results are discussed in the order in which they occurred, that is, Near-Earth tests, Null test, Deep-Space tests, and repetitive Near-Earth tests.

The sequence of testing and selected experimental results are shown in table II.

The Near-Earth (NE) tests were an approximate simulation of the heating environment encountered by a cryogenic vehicle in a "near-Earth" orbit. An exact simulation, of course, depends on many factors, including the vehicle attitude, its flight path, and the surface properties of the outer insulation surface, and can result in surface temperatures ranging between 167 K (300° R) and near room temperature. The 294 K (530° R) level selected for these tests is near the high end of the expected variation. It should also be noted that this temperature level could be representative of the temperatures experienced by a cryogenic vehicle in the cargo bay of the Space Shuttle. These tests, NE-1, NE-2, NE-3, and NE-4, were run first in order to determine the basic performance of the system prior to any major thermal cycling.

Following the NE tests was the null test, NU-1. This was accomplished by surrounding the entire vehicle with a 22 K (40° R) surface (e.g., see fig. 32). Its purpose was to determine if any unaccounted for heat leaks existed through the various plumbing, electrical, and instrumentation lines penetrating the tank insulation system. The Null test was performed prior to the Deep-Space tests and helped to ensure that the heat transfer rates measured for the Deep-Space tests were mostly a result of heating from the 294 K (530° R) payload.

The Deep-Space tests (designated "NS" in table II) were a simulation of the heating environment experienced by cryogenic tankage aboard a payload-to-sun-oriented vehicle (e.g., fig. 1) beyond the thermal influence of the Earth or other planetary bodies. A nearly similar heating environment would be encountered by a payload-to-sun-oriented cryogenic vehicle in synchronous orbit. This test involved holding the simulated payload at 294 K (530° R) while the remaining environment was held at 22 K (40° R). The Deep-Space tests, NS-1, NS-2, and NS-3, measured the heat transfer rates for three different vacuum chamber pressure levels. This was done because, at the low heating rates expected, gaseous conduction could be a major portion of the heat transfer to the system. The heating data at the three vacuum pressure levels used could thus provide a basis for possible extrapolation of the results to the much lower vacuum pressures expected in space.

After the Null and Deep-Space tests, which constituted a major thermal cycle of the entire tankage system, additional Near-Earth tests were made at two other vacuum pressure levels (NE-5 and NE-6). At this point the experimental package was removed to install the shadow shields (ref. 14) for further testing. The shadow shields had little or no effect on the subsequent Near-Earth tests shown. Test NE-7 is the first Near-Earth test with the shields applied. Between NE-7 and NE-8 were several Null and Deep-Space tests, which again represented a major thermal cycle of the system. The last four Near-Earth tests shown were an attempt to determine the pressure effects after thermal cycling.

Near-Earth Tests

Tests NE-1, NE-2, NE-3, and NE-4 represent the overall heat transfer rates measured at pressures in the low 1.3×10^{-3}-N/m^2 (10^{-5}-torr) range. This was about the lowest pressure achievable for this particular imposed test condition. Excluding test NE-2, which contained a planned electrical heat addition, the measured heat transfer rate is an average value of 22.7 watts (77.4 Btu/hr) for the entire hydrogen tank system. For a hydrogen tank vented at atmospheric pressure this represents only about 1.4 percent per day for the 4.96-cubic-meter (175.0-ft^3) tank used.

Table III is a breakdown of the overall heat transfer rates for tests NE-1 to NE-4. The results of the remaining Near-Earth tests (NE-5 to NE-11), included for completeness, are discussed later in this section. Item 1 of table III is the measured boiloff heat transfer rate. Item 2 is the effect of all the penetrations that would not be on a flight vehicle but that were necessary for experimental testing of the insulated tank. Item 3 is the Null-test heat trasfer rate. The measured boiloff minus the heat leaks due to experimentally necessary hardware and connections to the facility yields the expected in-flight heat transfer rate to the liquid hydrogen tank (item 4) for the flight surroundings simulated. Item 5 is the sum of the heat leak rates resulting from necessary flight vehicle tank penetrations, such as the fiberglass support struts, the vehicle plumbing, and the electrical leads. These heat leaks were determined from measured temperature gradients along the penetration as it entered the tankage system and the known physical characteristics of the penetration. Item 6 represents the total heat transferred through the insulation system.

Item 7, the sum of insulation blanket disturbance heat transfer rates, represents the penalties paid for the particular method of applying the MLI to the tank. In this case the penalties are the heat leakage through the nylon support pins, the area around the strut penetration, and the insulation seams. The conduction heat leakage through the support pins was determined from temperature measurements on the pin itself, along with the physical characteristics of the pin. The heat leakage resulting from penetration disturbances around the fiberglass strut (QPEN. EFFECTS) and the insulation seams (QSEAM) was determined in separate calorimeter tests, as reported in reference 23. In brief, reference 23 determined the effect of blanket disturbance (strut penetration or seam) by measuring the heat transfer rate through both an undisturbed blanket and a disturbed blanket. For the strut penetration the heat leakage through the strut itself was isolated experimentally in order to determine the net effect of the blanket disturbance. This net effect, when adjusted for the fact that the large insulated tank had pairs of adjacent struts (as opposed to a single strut used in ref. 23), was 1.05 watts (3.6 Btu/hr), as noted in reference 14. This value multiplied by six strut pairs yields the table results. Reference 23 states that the strut penetration disturbance

ranged between 1.05 and 0.68 watts (3.6 and 2.32 Btu/hr). The higher value is used in this report. Likewise reference 23 determined a seam heat leakage rate of 0.189 watt per meter (0.0164 Btu/hr in.). Applying the total seam length of 20.6 meters (810 in.) yields the results shown for the seams.

Item 8 of table III then represents an experimental estimate of the heat transferred through the undisturbed MLI. Item 9 gives the calculated results using the MLI correlation equation as reported in reference 24 and repeated here.

$$q = \frac{C_s \bar{N}^{2.56}}{N_s}\left(\frac{T_o + T_t}{2}\right)(T_o - T_t) + \frac{C_r \epsilon_{sh}}{N_s}\left(T_o^{4.67} - T_t^{4.67}\right) + \frac{C_p P}{N_s}\left(T_o^{0.26} - T_t^{0.26}\right) \qquad (6)$$

Finally item 10 of table III represents the percentage difference between the experimentally estimated MLI heat transfer and that determined by the semiempirical equation of reference 24.

The overall agreement between the experimentally determined and calculated values of heat transfer rate for the undisturbed insulation is good. Comparison is not as good when the lower value of strut penetration disturbance from reference 23 is used. This comparison, however, is somewhat academic since (1) the calculated value of heat transferred was based on several assumptions and (2) it is practically impossible to achieve these calculated rates for a real system. A more meaningful comparison would be to compare the total heat transferred through the applied insulation with that through the idealized undisturbed insulation (i.e., item 6 with item 9). Taking a ratio of these two heat transfer rates yields a factor of 2.6. This factor is the performance penalty paid for the method of insulation application and is as good or better than any experienced previously in the field (e.g., refs. 10, 13, and 15). Hence, the modularized nature of the insulation system developed and its inherent ease of application make it an attractive alternative for cryogenic Space Tug applications.

Another comparison that can be drawn is the relation of the overall measured boil-off heat transfer to that through the idealized undisturbed insulation (i.e., item 1 with item 9). This factor includes not only the performance penalty paid for the method of insulation application but also the detrimental effects of both the necessary flight configuration penetrations and the penetrations needed for testing operations and data collection. The ratio yields a factor of 3.0, which still compares favorably with the results of other investigations in the field.

Deep-Space Tests

Tests NS-1, NS-2, and NS-3 of table II are Deep-Space tests for three different pressure levels. The results of these tests are plotted in figure 33, along with the analytical results of reference 14, which uses the undisturbed insulation blanket correlation equation (eq. (6)). The experimental results are the measured boiloff heat transfer rates including penetrations, insulation disturbances, and so forth. As seen from table II the Null-test heat transfer rate is small and does not measurably affect the results. A detailed breakdown of the overall heat transfer rate for the Deep-Space tests is given in reference 14 and is not included here for brevity.

As seen from figure 33, the overall heat transfer rate is of the order of 0.98 watt (3.3 Btu/hr) or less for the low pressures anticipated in space. The ratio of overall measured boiloff heat transfer to that through the idealized insulation is seen to be less than 1.0 for the three test points shown. If both sets of data are extrapolated to pressure levels expected during an actual space flight, the curves tend to reverse in their relation to one another. This implies that for deep-space pressure levels the analysis will always predict lower heat transfer rates through just the undisturbed insulation than would be encountered for the entire tank-vehicle assembly.

Actual space heat fluxes into a vehicle liquid hydrogen tank equal to or less than those encountered in tests NS-1 to NS-3 will result from the preferential orientation of the vehicle payload toward the sun (along the centerline of fig. 1). With this orientation, the only major heat source is the 294 K (530^{o} R) payload. The insulation surface temperatures measured for NS-1 are given in figure 34. Temperatures are given as a function of radial position from the tank centerline. As seen, the highest temperatures were at the top of the tank directly below the payload and the lowest at the bottom of the tank, where no heat source is present. Agreement between the analytical and experimental data is good.

Repetitive Near-Earth Tests

The remaining Near-Earth tests, NE-5 to NE-11, represent additional tests performed on the insulated tank to determine any differences in performance following the Deep-Space tests and to determine the effect of vacuum pressure on heat transfer rates. To enable comparisons from test to test, table IV summarizes all Near-Earth tests. Close examination of table IV indicates a degradation in performance with time. For example, compare the results of tests NE-1 and NE-11. The reason for the apparent degradation is not immediately obvious. We suspected that the vacuum pressure within the insulation blankets was higher than that within the shroud volume. This thought will

be pursued in later paragraphs. Figure 35 plots the results of table IV. The data points (from column 4) are grouped according to data taken between major thermal cycles. Although the data are not conclusive, the performance does seem to degrade after every cycle.

Further evidence of performance degradation can be determined from table V. Table V gives the insulation temperatures at various locations for the Near-Earth tests. The temperature at any given common location tended to be lower for test NE-11 than for test NE-1 even though the shroud vacuum pressure decreased. For example, compare the readings of sensors HI-8, -9, -7, -6, and -19 for test NE-1 with those readings for test NE-11. Also, the insulation normal temperature profiles from these two tests are plotted in figure 36 along with the temperature profile through the insulation predicted by using equation (6).

Precluding a change in the insulation layer density, or an increase in the emissivity of the radiation shields, the decrease in insulation temperature could indicate that the pressure within the insulation was higher than that indicated by the shroud pressure ion gage. Also note from table V the similarity of the temperature profiles and heat transfer rates for tests NE-8 and NE-11. The temperature profiles are practically identical, as are the measured heat transfer rates (table IV), despite the factor of 2 difference in shroud pressure. These factors indicate that the pressure within the insulation was not necessarily a function of shroud pressure.

Selected data taken both during approach to steady-state conditions and during a short tank lockup period indicate two possible sources of gas leakage beneath the insulation. One seemed to be related to the refilling of the cold guard tank and/or the liquid hydrogen tank and the other was a helium leak originating from the helium-operated vent valve located in the insulated tank valve box.

Figure 37 shows the temperature at various points on the insulation, mostly on the innermost surface, during approach to steady-state conditions for test NE-7. The temperatures steadied out prior to filling of the tank and cold guard, dipped slightly, then rose sharply after the filling operation, and eventually diminished to the prefilling values. The slight dip was probably caused by a temporary increase in pressure. The sharp increase in temperatures could only be brought about by a lower pressure within the inner layers of the insulation. Temperature measurements recorded during this period for the outer surface of the insulation, as well as for the tank fiberglass support struts, showed no change at all. Hence, the temporary pressure rise followed by the decrease was local; the data in hand suggest that the changes originated in the tank valve-box duct volume. The temperature data suggest that a leak was opened at the start of the filling operation, then closed, and then slowly reopened with time. It is interesting to note that the temperature levels that sensors HI-8, HI-9, HI-10, and P-7 (see fig. 31 for location) approached around 18 to 22 hours closely agree with those

measured initially during test NE-1 when the MLI blankets heat transfer rates were significantly lower. Sensors HI-33 and HI-34, both on the inner layer, also show significant temperature increases but cannot be compared to test NE-1 because they were added after the test program began (just before test NE-7).

Other evidence gathered, shown in figure 38, suggests that a gaseous helium leak was emanating from the helium-operated vent valve. (These data were taken immediately following steady state for the gaseous helium bleed test, NE-9.) The vent valve was maintained in the open position by applying 345 N/cm^2 (500 psig) of helium to the valve operator. The vent valve was closed by removing the helium pressure. This particular valve was located within the valve box, and its leakage obviously affected the insulation temperatures and performance. From figure 38 it is apparent that several insulation and component temperatures were measurably affected by closing the vent valve, that is, removing the 345 N/cm^2 (500 psig) on the operator. For example, insulation temperatures HI-9 and HI-10 increased, indicating a lower pressure within the insulation. Temperatures P-2, P-3, P-6, and P-7 all increased, which can only be explained by a decrease in pressure. Temperature P-8, on the fill line, decreased. This also was expected since the line received less heat transfer from the warmer surroundings of the cold guard duct because convective heat transfer was reduced as the pressure decreased. The line cooled because it was directly connected to the liquid hydrogen tank and ran through the cold guard tank.

Insulation temperature changes were less during the refilling of the cold guard tank after test NE-9 then they were during the refilling before test NE-7. The authors attribute this to the higher pressure existing within the shroud volume for test NE-9 than for test NE-7 (i.e., 7.9×10^{-3} as opposed to 4.8×10^{-3} N/m^2 (5.9×10^{-5} as opposed to 3.6×10^{-5} torr)). Again, as was the case during the refilling of the cold guard tank before test NE-7, temperature measurements recorded for the outer surface of the insulation as well as for the tank fiberglass support struts, showed no change at all during the period after test NE-9.

The influence of decreasing the helium leakage (by closing the vent valve) is felt even though the test pressure was at a relatively high level (i.e., 7.9×10^{-3} N/m^2 (5.9×10^{-5} torr)). It is not known if this leak persisted at the beginning of the test program (NE-1) or what influence it had on the results. If anything, its absence could have resulted in lower heat transfer rates. Likewise, the overall effect of the apparent opening and/or closing of a leak source during cold guard and tank refilling operations, is not conclusively known. However, the data from figure 35, grouped according to major thermal cycles of the system and/or chronological time, seem to indicate a degradation of insulation performance with time. From the available data, we believe that this degradation in performance is most likely a result of a leakage of gas beneath the insulation rather than a basic degradation in the MLI properties.

SUMMARY OF RESULTS AND CONCLUDING REMARKS

A multilayer insulation (MLI) system for a 2.23-meter-diameter (87.6-in.-diam) liquid hydrogen tank was designed, fabricated, and tested under conditions simulating a near-Earth orbital environment and a deep-space environment. The ground rules used to arrive at the particular design were as follows:

(1) The system must be rugged in order to minimize any degradation in thermal performance from handling.

(2) It must be modular so that part or all of the system can be easily removed or replaced.

(3) Substantial baseline performance data must be available in order to evaluate the penalties involved in applying a system.

(4) The performance of the system should be adequate for both reasonable ground-hold and near-Earth heat fluxes (e.g., 631 and 2.21 W/m^2 (<200 and 0.7 $Btu/hr\ ft^2$), respectively).

(5) The system should give repeatable performance from test to test.

The MLI system selected consisted of two insulation blankets each made up of alternate layers of double silk net (16 layers) and double-aluminized Mylar radiation shields (15 layers) contained between two cover sheets of Dacron-scrim-reinforced Mylar. The assembled layers of spacers, radiation shields, and cover sheets were held together by nylon button pins and retainers spaced every 20 centimeters (8 in.) throughout the blanket. The surfaces of both the button pins and the retainers adjacent to the cover sheets were cemented in place in order to provide a positive means of layer density control for the MLI. Nominal layer density of the insulation based on the button-pin-to-retainer dimension was 17.7 layers per centimeter (45 layers/in.). Where possible, all components were formed to the contours required to facilitate insulation assembly and to help maintain a uniform MLI density.

The insulation system was modularized in order to facilitate removal and/or replacement of insulation elements. In general, butt joints (with the cover sheet overlap on each side) or simple overlap joints were used. Velcro fasteners were used between the MLI blankets as well as to assemble the blankets onto the liquid hydrogen tank. The MLI system applied to the liquid hydrogen tank weighed approximately 23 kilograms (50.8 lb), that is, 1.54 kg/m^2 (0.32 lb/ft^2), including the fiberglass polar caps and valve box. The fiberglass components weighed 3.9 kilograms (8.6 lb).

Some general observations were made during the fabrication of the insulation system:

(1) The silk net spacers were easily formed by water soaking and subsequent air drying. The formed spacers simplified insulation assembly by eliminating the cutting

and darting of the spacer usually required and as an overall result yielded a more uniform-density insulation.

(2) Attempts to thermal vacuum form the aluminized Mylar radiation shields to the tank contour were unsuccessful because the shield emissivity was severely degraded in the highly stretched areas.

(3) Thermal vacuum forming of the Schjeldahl X-850 cover sheets was partially successful. Some springback in the material was experienced. Final forming was done with a hand iron to the desired contour.

Some general observations were made during application of the insulation to the liquid hydrogen tank:

(1) The modular nature of the insulation system greatly eased the application of the insulation.

(2) Using nylon positioning pins along with Velcro attachments provided a positive rapid means of applying and reapplying the insulation in a consistent manner.

(3) The insulation blankets as developed are rugged and can be applied and reapplied with no noticeable damage.

The insulated tank was tested at environmental conditions simulating both near-Earth orbital and deep-space conditions. The results of the Near-Earth tests were as follows:

1. The average overall heat transferred to the insulated liquid hydrogen tank from a hot-side boundary temperature of 294 K (530° R) was about 22.7 watts (77.4 Btu/hr).

2. Heat transferred through the various insulation penetrations such as the support struts, plumbing lines, and electrical wires amounted to about 3.2 watts (11 Btu/hr), leaving about 19.3 watts (66 Btu/hr) chargeable to the insulation. This represents about 1.29 W/m^2 (0.41 Btu/hr ft^2) for the 1.9-centimeter-thick (0.75-cm-thick) 34-layer system.

3. The heat transferred through the insulation as applied was approximately 2.6 times that predicted for a "perfectly" applied system (i.e., no seams or penetrations in the insulation). This performance is equal to or better than for other complete tank systems previously tested.

4. Repetitive testing of the system showed some degradation in insulation performance with time. Experimental evidence suggests that the degradation was probably a result of unplanned leakage of gases beneath the insulation system rather than a basic degradation in the insulation properties. Although not conclusive, the few tests repeated under conditions similar to a Space Tug application (i.e., evacuated tests interspersed by warmups and exposure to atmospheric conditions) disclose that the insulation system has definite possibilities for reusability.

The results of the Deep-Space tests were as follows:

1. The heat transfer rate for the insulated liquid hydrogen exposed to a 294 K

(530° R) payload only was 0.98 watt (3.3 Btu/hr) for the lowest vacuum pressure obtained, that is, 8×10^{-4} N/m^2 (6×10^{-6} torr).

2. The temperature profile of the insulation surface varied from 159 K (287° R) nearest the payload to 67 K (121° R) at the equator and 26 K (47° F) at the bottom of the tank and agreed quite well with the analytical prediction.

Overall, the modular insulation system as developed was rugged and easily applied (or replaced) and performed very well considering the simplified seams and attachment methods used. The performance level of the system shows that this concept may be useful for a cryogenic Space Tug or orbit transfer vehicle application.

Lewis Research Center,
National Aeronautics and Space Administration,
Cleveland, Ohio, July 14, 1976,
506-21.

APPENDIX - SYMBOLS

A	area, m^2; ft^2
C_s	constant, 4.89×10^4 $cm^{2.56}$ W/(layers$^{2.56}$ K^2 m^2); 1.33×10^4 $in.^{2.56}$ Btu/(layers$^{2.56}$ R^2 hr ft^2)
C_r	constant, 5.39×10^{-10} W/($K^{4.67}$ m^2); 1.10×10^{-11} Btu/($^oR^{4.67}$ hr ft^2)
C_p	constant, 6.71×10^{-10} W/(N/m^2 $K^{0.26}$ m^2); 8.06×10^{-10} Btu/($^oR^{0.26}$ torr hr ft^2)
DINSUL	energy-content change of insulation system, W; Btu/hr
DLIQUID	energy-content change of test-tank liquid, W; Btu/hr
DTANK	energy-content change of test-tank wall, W; Btu/hr
DULLAGE	energy-content change of test-tank ullage, W; Btu/hr
h	specific enthalpy, J/kg; Btu/lb
k	thermal conductivity, W/m K; Btu/hr ft ^oR
L	length or thickness, m; ft
$\dot{M}$	mass flow rate, kg/hr; lb/hr
$\bar{N}$	insulation layer density, layers/cm; layers/in.
N_s	number of insulation sheets, dimensionless
P	pressure, N/m^2 (torr)
Q	heat flow, W; Btu/hr
QBLKTS	heat transferred through uninterrupted insulation blankets, W; Btu/hr
QBOILOFF	latent and sensible heat content of boiloff gases, W; Btu/hr
QDUCT	heat added to tank by conduction through valve box and by radiation from duct volume, W; Btu/hr
QPEN. EFFECTS	increased heat transfer through insulation blankets due to penetration of fiberglass struts, W; Btu/hr
QPINS	heat added by solid conduction through nylon positioning pins, W; Btu/hr
QPLUMBING	heat added by solid conduction through service lines and tubes connected to test tank, W; Btu/hr

QSEAM	increased heat transfer through insulation blanket system due to presence of seams between blankets, W; Btu/hr
QSTRUTS	heat added by conduction down fiberglass struts, W; Btu/hr
QWIRES	heat added by conduction through instrumentation and control wires, W; Btu/hr
q	heat flux, W/m^2; Btu/ft^2 hr
T	temperature, K; ^oR
$\dot{V}$	volumetric flow, m^3/hr; ft^3/hr
ϵ	total hemispherical emittance
λ	latent heat of evaporation, J/kg; Btu/lb
ρ	density, kg/m^3; lb/ft^3
σ	Stefan-Boltzmann constant, 5.668×10^{-8} W/m^2 K^4; 1.713×10^{-9} Btu/hr ft^2 R^4

Subscripts:

bo	boiloff
cond	conduction
liq	liquid
o	outside surface of insulation
rad	radiation
sh	insulation sheet
stp	standard temperature and pressure
sv	saturated vapor
t	tank
tv	tank vent
w	wall

REFERENCES

1. Knoll, R. H.; and Oglebay, J. C.: Lightweight Thermal Protection Systems for Space Vehicle Propellant Tanks. SAE Paper 746C, Sept. 1963.

2. Knoll, Richard H.; and Bartoo, Edward R.: Experimental Studies on Shadow Shields for Thermal Protection of Cryogenic Tanks in Space. NASA TN D-4887, 1968.

3. Boyle, Robert J.; and Knoll, Richard H.: Thermal Analysis of Shadow Shields and Structural Members in a Vacuum. NASA TN D-4876, 1968.

4. Titan/Centaur T/C-1 Post Flight Evaluation Report. NASA TM X-71692, 1975.

5. Westmoreland, L. Q.; Space Tug Systems Study (Cryogenic). Volume 2; Technical Compendium. MDC-G5029-Vol-2, McDonnell Douglas Corp.; NAS8-29677) NASA CR-120460, 1974.

6. Cohan, C. J.; Peters, C. F.; and Jones, D. J.: Space Tug Systems Study (Cryogenic). CASD-NAS73-033-Vol-2, General Dynamics Convair Aerospace Div. (NAS8-29676), 1974.

7. Advanced Studies on Multilayer Insulation Systems. (ADL-67180-00-04, Arthur D. Little, Inc.; NAS3-6283) NASA CR-54929, 1966.

8. Keller, C. W.: Thermal Performance of Multilayer Insulation. (LMSC-A974469, Lockheed Missiles & Space Co.; NAS3-12025) NASA CR-72747, 1971.

9. Sterbentz, W. H.; and Baxter, J. W.: Thermal Protection System for a Cryogenic Spacecraft Propulsion Module, Volume II. (LMSC-A794993, Vol. II, Lockheed Missiles & Space Co.; NAS3-4199) NASA CR-54879, 1966.

10. Leonhard, K. E.; and Hyde, E. H.: Flightworthy, High Performance Insulation Development. Cryogenic Technol., vol. 7, no. 4, July/Aug. 1971, pp. 115-118.

11. Nies, G. E.: Lightweight Modular Multi-layer Insulation. (Union Carbide Corp.; NAS3-12045) NASA CR-72856, 1971.

12. Fredrickson, G. O.: Investigation of High-Performance Insulation Application Problems. (MDC-G4722, McDonnell Douglas Astronautics Co.; NAS8-21400) NASA CR-124400, 1973.

13. Walburn, A. B.: Development of a Reusable Flightweight Cryogenic Storage System. AIAA Paper 74-726, July 1974.

14. DeWitt, Richard L.; and Boyle, Robert J.: Thermal Performance of an Integrated Thermal Protection System for Long-Term Storage of Cryogenic Propellants in Space. NASA TN D-8320, 1977.

15. DeWitt, Richard L.; and Mellner, Max B.: Experimental Evaluation of a Purged Substrate Multilayer Insulation System for Liquid Hydrogen Tankage. NASA TN D-6331, 1971.

16. Sumner, Irving E.; and Maloy, Joseph E.: Transient Thermal Performance of Multilayer Insulation Systems During Simulated Ascent Pressure Decay. NASA TN D-6335, 1971.

17. Stochl, Robert J.: Basic Performance of a Multilayer Insulation System Containing 20 to 160 Layers. NASA TN D-7659, 1974.

18. Leonhard, K. E.: Cryogenic Insulation Development. (GDCA-DDB72-004, General Dynamics/Convair; NAS8-26129) NASA CR-123938, 1972.

19. Lofgren, C. L.; and Gieseking, D. E.: Multilayer Insulation Panels. (The Boeing Co.; NAS3-14179) NASA CR-72857, 1971.

20. Carter, J. S.; and Timberlake, T. E.: Filament-Wound, Fiberglass Cryogenic Tank Supports. BC-8367-FR, Brunswick Corp.; NAS3-14627) NASA CR-120828, 1971.

21. Kirchmeier, W. E., Jr.: System Accurately Controls Pressure in Cryogenic Tanks. NASA Tech Brief B71-10118, 1971.

22. Santeler, Donald J., et al.: Vacuum Technology and Space Simulation. NASA SP-105, 1966.

23. Sumner, I. E.: Degradation of a Multilayer Insulation due to a Seam and a Penetration. NASA TN D-8229, 1976.

24. Keller, C. W.; Cunnington, G. R.; and Glassford, A. P.: Thermal Performance of Multilayer Insulations. (LMSC-D349866, Lockheed Missile & Space Co.; NAS3-14377) NASA CR-134477, 1974.

TABLE I - DESIGN DATA FOR MLI BLANKET MATERIALS

Item	Material	Room-temperature emissivity	Unit weight	
			g/cm^2	lb/ft^2
Radiation shield	0.0064-mm (1/4-mil) double-aluminized Mylar	<0.04 on both sides	0.000884	0.00181
Shield spacer	4.7×7.1 Mesh per cm^2 (12×18 mesh/$in.^2$) silk net of thickness ≤0.010 cm (≤0.004 in.)	----------	≤0.000732[a]	≤0.0015[a]
Blanket cover sheet	Schjeldahl X-850, which is a laminate of	≤0.05 on both sides	0.0078	0.016
	(a) 0 0064-mm (1/4-mil) single-aluminized Mylar	≤0 05 on aluminized surface	.000884	00181
	(b) Dacron scrim	----------	0020	.00419
	(c) 0 013-mm (1/2-mil) single-aluminized Mylar	≤0.05 on aluminized surface	00177	.00362

[a]Per single layer.

TABLE II - DESCRIPTION AND CHRONOLOGY OF THERMAL TESTS

Test designation	Test condition	Area-weighted payload temperature		Area-weighted shroud temperature		Original, recorded, shroud-volume ion gage reading		Corrected shroud-volume ion gage reading		Test purpose	Duration of steady state, hr	Total measured heat transfer rate	
		K	°R	K	°R	N/m^2	torr	N/m^2	torr			W	Btu/hr
NE-1	Near Earth	295	531	295 5	532	$4\ 5\times10^{-4}$	$3\ 4\times10^{-6}$	$2\ 3\times10^{-3}$	$1\ 7\times10^{-5}$	Baseline	14	22 5	76 9
NE-2	Near Earth	297	534	297	534	$4\ 5\times10^{-4}$	3.4×10^{-6}	$2\ 3\times10^{-3}$	$1\ 7\times10^{-5}$	Effect of heat addition	2	27 3	93.1
NE-3	Near Earth	296	533	295 5	532	4.5×10^{-4}	$3\ 4\times10^{-6}$	$2\ 1\times10^{-3}$	$1\ 6\times10^{-5}$	Repeat after heat addition	8	22 4	76 6
NE-4	Near Earth	294.5	530	295.5	532	2.9×10^{-4}	2.2×10^{-6}	1.5×10^{-3}	$1\ 1\times10^{-5}$	Repeat after tank retopping	12	23.0	78 6
Shroud failure and repair													
NU-1	Null	23 .5	42	23	41	$1\ 7\times10^{-3}$	1.3×10^{-5}	9.6×10^{-3}	$7\ 2\times10^{-5}$	Effect of facility	18	0 041	0 14
NS-1	Deep Space	286 5	516	23 5	42	1.3×10^{-3}	$1\ 0\times10^{-5}$	7.9×10^{-3}	5.9×10^{-5}	Baseline	17	.98	3 33
NS-2	Deep Space	286.5	516	23	41	6.3×10^{-3}	$4\ 7\times10^{-5}$	3.6×10^{-2}	2.7×10^{-4}	Effect of pressure (gaseous helium bleed)	9	1.44	4.93
NS-3	Deep Space	286.5	516	23	41	1.6×10^{-2}	1.2×10^{-4}	9.3×10^{-2}	$7\ 0\times10^{-4}$	Effect of pressure (gaseous helium bleed)	21	2.18	7 46
NE-5	Near Earth	296	533	297	534	1.6×10^{-3}	$1\ 2\times10^{-5}$	7.5×10^{-3}	$5\ 6\times10^{-5}$	Repeat after Deep Space	19	26 1	89 1
NE-6	Near Earth	295 5	532	297	534	1.0×10^{-2}	7.7×10^{-5}	4.9×10^{-2}	$3\ 7\times10^{-4}$	Effect of pressure (gaseous helium bleed)	(a)	46.1	157.5
Shields added to vehicle													
NE-7	New Earth	294 5	530	295 5	532	1.1×10^{-3}	8.0×10^{-6}	4.8×10^{-3}	$3\ 6\times10^{-5}$	Verify hardware integrity	23	25 7	87 6
Several Null and Deep-Space tests with shadow shields													
NE-8	Near Earth	294	529	295	531	3.7×10^{-4}	2.8×10^{-6}	1.9×10^{-3}	$1\ 4\times10^{-5}$	Repeat after Deep Space	15	25 5	87 2
NE-9	Near Earth	294	529	295	531	1.6×10^{-3}	$1\ 2\times10^{-5}$	7.9×10^{-3}	5.9×10^{-5}	Effect of pressure (gaseous helium bleed)	11	34 7	118 5
NE-10	Near Earth	293.5	528	295.5	532	8.1×10^{-3}	6.1×10^{-5}	4.0×10^{-2}	$3\ 0\times10^{-4}$	Effect of pressure (gaseous helium bleed)	11	80.4	274.6
NE-11	Near Earth	294	529	295	531	1.7×10^{-4}	1.3×10^{-6}	8.7×10^{-4}	$6\ 5\times10^{-6}$	Repeat of test NE-7	18	25 6	87 5

[a]Short-time test, steady state not achieved for all parameters

TABLE III - SUMMARY OF HEAT TRANSFER RATES FOR NEAR-EARTH TESTS

Item	Heat transfer term	Test										
		Minimum pressure - no gaseous helium bleed					Bleed	No bleed		Bleed		No bleed
		NE-1	NE-2	NE-3	NE-4	NE-5	NE-6	NE-7	NE-8	NE-9	NE-10	NE-11
		Shroud vacuum pressure, N/m^2 (torr)										
		2.3×10^{-3} (1.7×10^{-5})	2.3×10^{-3} (1.7×10^{-5})	2.1×10^{-3} (1.6×10^{-5})	1.5×10^{-3} (1.1×10^{-5})	7.5×10^{-3} (5.6×10^{-5})	4.9×10^{-2} (3.7×10^{-4})	4.8×10^{-3} (3.6×10^{-5})	1.9×10^{-3} (1.4×10^{-5})	7.9×10^{-3} (5.9×10^{-5})	4.0×10^{-2} (3.0×10^{-4})	8.7×10^{-4} (6.5×10^{-6})
		Steady-state heat transfer rate, W (Btu/hr)										
1	Measured boiloff heat transfer rate	22.5 (76.9)	27.3 (93.1)	22.4 (76.6)	23.0 (78.6)	26.1 (89.1)	46.1 (157.5)	25.7 (87.6)	25.5 (87.2)	34.7 (118.5)	80.4 (274.6)	25.6 (87.5)
	Nonflight measured heat transfer rates											
	Electric power to resistor	------ ------	3.9 (13.5)	------ ------	------ ------	------ ------	------- -------	------ ------	------ ------	------- -------	------ ------	------ ------
	Duct	0.5 (1.6)	.5 (1.6)	.5 (1.6)	0.5 (1.6)	0.4 (1.3)	0.3 (1.0)	0.4 (1.3)	0.3 (1.1)	0.3 (1.1)	0.3 (1.1)	0.4 (1.2)
	Plumbing lines and electrical wires	0 (0)	0 (0)	0 (0)	0 (0)	.03 (.1)	.03 (.1)	.03 (.1)	.03 (.1)	.03 (.1)	.03 (.1)	.03 (.1)
2	Sum of nonflight heat transfer rates	.5 (1.6)	4.4 (15.1)	.5 (1.6)	.5 (1.6)	.4 (1.4)	.3 (1.1)	.4 (1.4)	.4 (1.2)	.4 (1.2)	.4 (1.2)	.4 (1.3)
3	Null heat transfer rate	0.1 (.2)	0.1 (.2)	0.1 (.2)	0.1 (.2)	0.1 (.2)	0.1 (.3)	0.1 (.2)	0.1 (.2)	0.1 (.2)	0.1 (.2)	0.1 (.2)
4	Heat transfer rate to flight liquid hydrogen tank (items 1-2-3)	22.0 (75.1)	22.8 (77.8)	21.9 (74.8)	22.5 (76.8)	25.6 (87.5)	45.7 (156.1)	25.2 (86.0)	25.1 (85.8)	34.3 (117.1)	80.0 (273.2)	25.2 (86.0)
	Measured noninsulation heat transfer rates											
	Struts	2.0 (6.8)	2.0 (6.8)	2.0 (6.8)	2.0 (6.8)	1.9 (6.6)	2.0 (6.9)	2.0 (6.8)	2.0 (6.8)	2.1 (7.2)	2.5 (8.6)	2.0 (6.9)
	Electrical wires	.4 (1.3)	.4 (1.3)	.4 (1.3)	.4 (1.3)	.4 (1.3)	.4 (1.3)	.4 (1.3)	.4 (1.2)	.4 (1.2)	.4 (1.2)	.4 (1.3)
	Plumbing lines	.4 (1.4)	.4 (1.4)	.4 (1.4)	.2 (.6)	.1 (.5)	.2 (.6)	.2 (.6)	.1 (.5)	.2 (.6)	.1 (.2)	-.1 (-.4)
5	Sum of noninsulation heat transfer rates	2.8 (9.5)	2.8 (9.5)	2.8 (9.5)	2.5 (8.7)	2.5 (8.4)	2.6 (8.8)	2.5 (8.7)	2.5 (8.5)	2.6 (9.0)	2.9 (10.0)	2.3 (7.8)
6	Heat transfer rate through insulation (items 4-5)	19.2 (65.6)	20.0 (68.3)	19.1 (65.3)	19.9 (68.1)	23.2 (79.1)	43.1 (147.3)	22.6 (77.3)	22.6 (77.3)	31.7 (108.1)	77.1 (263.2)	22.9 (78.2)
	Measured insulation heat transfer rates											
	Pins	2.0 (6.8)	2.0 (6.8)	2.0 (6.8)	2.0 (6.8)	1.9 (6.4)	1.8 (6.1)	1.8 (6.3)	1.7 (5.9)	1.4 (4.9)	1.2 (4.0)	1.7 (5.9)
	Seam effect	3.9 (13.3)	3.9 (13.3)	3.9 (13.3)	3.9 (13.3)	3.9 (13.3)	8.8 (29.9)	3.9 (13.3)	3.9 (13.3)	6.4 (21.9)	15.6 (53.4)	3.9 (13.3)
	Penetration effect	6.3 (21.6)	6.3 (21.6)	6.3 (21.6)	6.3 (21.6)	6.3 (21.6)	6.3 (21.6)	6.3 (21.6)	6.3 (21.6)	6.3 (21.6)	6.3 (21.6)	6.3 (21.6)
7	Sum of disturbances to insulation blanket	12.2 (41.7)	12.2 (41.7)	12.2 (41.7)	12.2 (41.7)	12.1 (41.3)	16.9 (57.6)	21.1 (41.2)	11.9 (40.8)	14.2 (48.4)	23.1 (79.0)	11.9 (40.8)
8	Blanket heat transfer rate (items 6-7)	7.0 (23.9)	7.8 (26.6)	6.9 (23.6)	7.7 (26.4)	11.1 (37.8)	26.3 (89.7)	10.6 (36.1)	10.7 (36.5)	17.5 (59.7)	53.9 (184.2)	11.0 (37.4)
9	Blanket correlation, eq (6)	7.6 (25.8)	7.6 (26.0)	7.6 (25.9)	7.2 (24.7)	9.4 (32.1)	23.9 (81.5)	8.4 (28.8)	7.3 (24.8)	9.3 (31.9)	20.1 (68.5)	6.9 (23.7)
10	Difference (items [(8-9)/9]×100), percent	-7.4	2.3	-8.9	6.9	17.8	10.1	25.3	47.2	87.1	168.9	57.8

TABLE IV. - SUMMARY OF NEAR-EARTH TESTS

Test	Corrected shroud pressure		Measured heat transfer rate		Heat transfer rate through insulation[a]		Blanket heat transfer rate		Blanket correlation (eq. (6))	
	N/m^2	torr	W	Btu/hr	W	Btu/hr	W	Btu/hr	W	Btu/hr
NE-1	2.3×10^{-3}	1.7×10^{-5}	22.5	76.9	19.2	65.6	7.0	23.9	7.6	25.8
NE-2	2.3×10^{-3}	1.7×10^{-5}	27.3	93.1	20.0	68.3	7.8	26.6	7.6	26.0
NE-3	2.1×10^{-3}	1.6×10^{-5}	22.4	76.6	19.1	65.3	6.9	23.6	7.6	25.9
NE-4	1.5×10^{-3}	1.1×10^{-5}	23.0	78.6	19.9	68.1	7.7	26.4	7.2	24.7
First major cold shock (Null and Deep-Space tests)										
NE-5	7.5×10^{-3}	5.6×10^{-5}	26.1	89.1	23.2	79.1	11.1	37.8	9.4	32.1
NE-6	4.9×10^{-2}	3.7×10^{-4}	46.1	157.5	43.1	147.3	26.3	89.7	23.9	81.5
Addition of shadow shields										
NE-7	4.8×10^{-3}	3.6×10^{-5}	25.7	87.6	22.6	77.3	10.6	36.1	8.4	28.8
Second major cold shock (Null and Deep-Space tests)										
NE-8	1.9×10^{-3}	1.4×10^{-5}	25.5	87.2	22.6	77.3	10.7	36.5	7.3	24.8
NE-9	7.9×10^{-3}	5.9×10^{-5}	34.7	118.5	31.7	108.1	17.5	59.7	9.3	31.9
NE-10	4.0×10^{-2}	3.0×10^{-4}	80.4	274.6	77.1	263.2	53.9	184.2	20.1	68.5
NE-11	8.7×10^{-4}	6.5×10^{-6}	25.6	87.5	22.9	78.2	11.0	37.4	6.9	23.7

[a]Measured heat transfer rate less heat transferred through penetrations (same as item 6 in table III)

TABLE V - SUMMARY OF INSULATION TEMPERATURES FOR NEAR-EARTH TESTS

Sensor	Location	Cover sheet	Layer	Test										
				NE-1	NE-2	NE-3	NE-4	NE-5	NE-6	NE-7	NE-8	NE-9	NE-10	NE-11
				Corrected shroud pressure, N/m^2 (torr)										
				$2\ 3\times10^{-3}$ ($1\ 7\times10^{-5}$)	$2\ 3\times10^{-3}$ ($1\ 7\times10^{-5}$)	$2\ 1\times10^{-3}$ ($1\ 6\times10^{-5}$)	$1\ 5\times10^{-3}$ ($1\ 1\times10^{-5}$)	$7\ 5\times10^{-3}$ ($5\ 6\times10^{-5}$)	$4\ 9\times10^{-2}$ ($3\ 7\times10^{-4}$)	$4\ 8\times10^{-3}$ ($3\ 6\times10^{-5}$)	$1\ 9\times10^{-3}$ ($1\ 4\times10^{-5}$)	$7\ 9\times10^{-3}$ ($5\ 9\times10^{-5}$)	$4\ 0\times10^{-2}$ ($3\ 0\times10^{-4}$)	$8\ 7\times10^{-4}$ ($6\ 5\times10^{-6}$)
				Temperature, K (^{o}R)										
-----	Outer layer (average)[a]	Outer	34	293 (527)	293 (528)	293 (528)	292 (526)	293 (528)	292 (526)	292 (526)	291 (524)	291 (523)	288 (519)	291 (524)
	Outer blanket gore panel													
HI-5	Center of panel	Outer	34	293 (528)	293 (528)	293 (528)	293 (527)	293 (528)	292 (526)	292 (526)	292 (526)	291 (524)	289 (521)	292 (526)
HI-6	Center of panel	Inner	18	257 (462)	257 (463)	257 (463)	257 (462)	254 (458)	252 (453)	254 (458)	251 (451)	231 (415)	178 (320)	251 (451)
HI-17	Upper half - near edge	Outer	34	292 (526)	293 (527)	293 (527)	292 (526)	293 (527)	291 (524)	291 (524)	291 (523)	290 (522)	288 (518)	291 (523)
HI-18	Upper half - near edge	Inner	18	246 (443)	246 (443)	247 (444)	246 (443)	242 (435)	238 (428)	239 (431)	234 (422)	212 (381)	165 (297)	234 (422)
HI-19	Upper half - at edge	Inner	18	253 (456)	254 (457)	254 (457)	253 (456)	249 (449)	246 (443)	246 (442)	243 (437)	227 (408)	195 (351)	243 (437)
HI-20	Positioning pin cover		28	278 (500)	278 (500)	278 (500)	277 (499)	278 (500)	276 (496)	275 (495)	276 (496)	273 (492)	267 (481)	276 (496)
	Inner blanket gore panel													
HI-7	Center of panel	Outer	17	252 (454)	252 (454)	252 (454)	252 (454)	----- -----	----- -----	249 (449)	245 (441)	223 (401)	168 (303)	245 (441)
HI-8	Center of panel	Inner	1	76 (137)	77 (138)	77 (138)	76 (137)	49 (89)	29 (53)	51 (92)	43 (78)	31 (55)	28 (50)	44 (79)
HI-9	Upper half - at edge			104 (188)	105 (189)	105 (189)	106 (190)	92 (166)	54 (97)	89 (160)	81 (146)	47 (85)	32 (58)	84 (151)
HI-31	Lower half - on flap			----- -----	----- -----	----- -----	----- -----	----- -----	----- -----	27 (48)	26 (47)	25 (45)	25 (45)	27 (48)
HI-32	Lower half - at edge			----- -----	----- -----	----- -----	----- -----	----- -----	----- -----	37 (66)	31 (56)	27 (49)	24 (44)	32 (57)
HI-33	Lower half - near edge			----- -----	----- -----	----- -----	----- -----	----- -----	----- -----	40 (72)	31 (55)	22 (39)	21 (37)	31 (56)
HI-34	Lower half - middle			----- -----	----- -----	----- -----	----- -----	----- -----	----- -----	38 (69)	28 (51)	22 (39)	19 (35)	29 (52)
HI-22	Upper polar fiberglass cap	------	0	144 (260)	144 (260)	145 (261)	145 (261)	136 (245)	119 (214)	----- -----	----- -----	----- -----	----- -----	----- -----
HI-10	Fiberglass valve-box lid	------	0	107 (193)	107 (193)	108 (194)	107 (193)	94 (170)	82 (148)	92 (166)	79 (142)	74 (134)	68 (123)	82 (148)
P-7	Fiberglass valve-box side	------	0	91 (163)	91 (164)	91 (164)	92 (165)	76 (137)	71 (127)	70 (126)	61 (110)	58 (105)	57 (103)	64 (115)

[a]Average of HI-23, HI-2, HI-1, HI-30, HI-15, HI-4, HI-16, HI-17, HI-5, HI-12, HI-13, HI-14, and HI-3

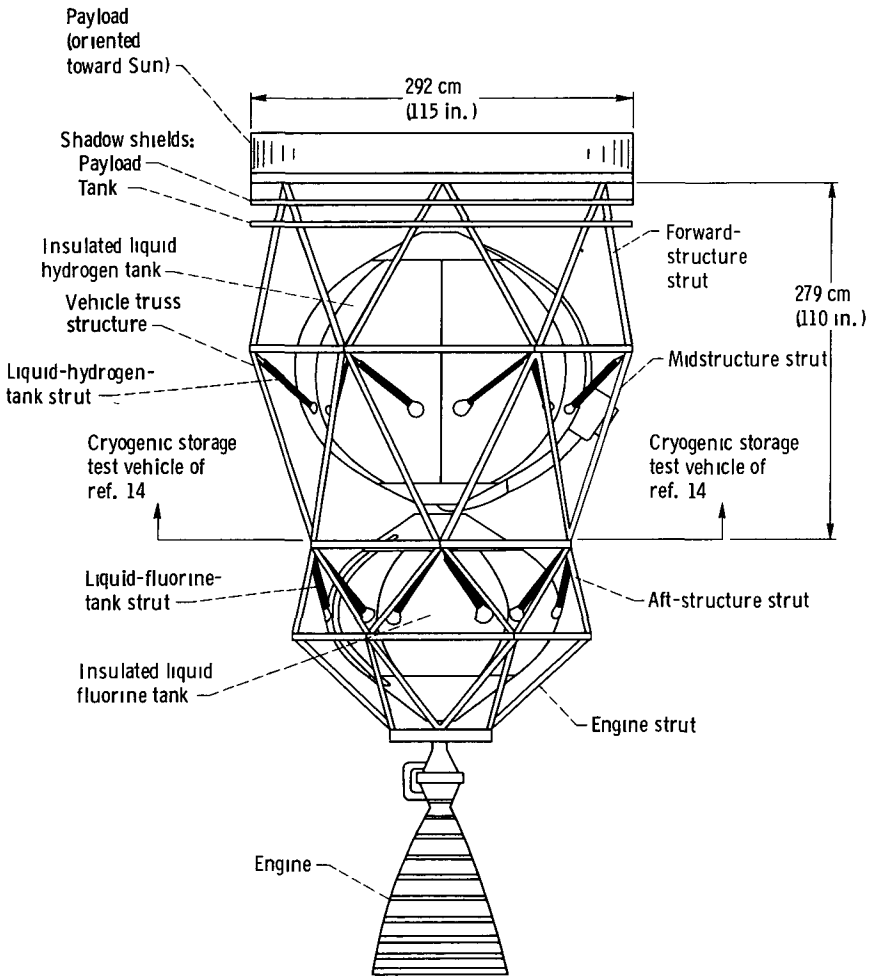

Figure 1. - Conceptual design of hydrogen-fluorine stage.

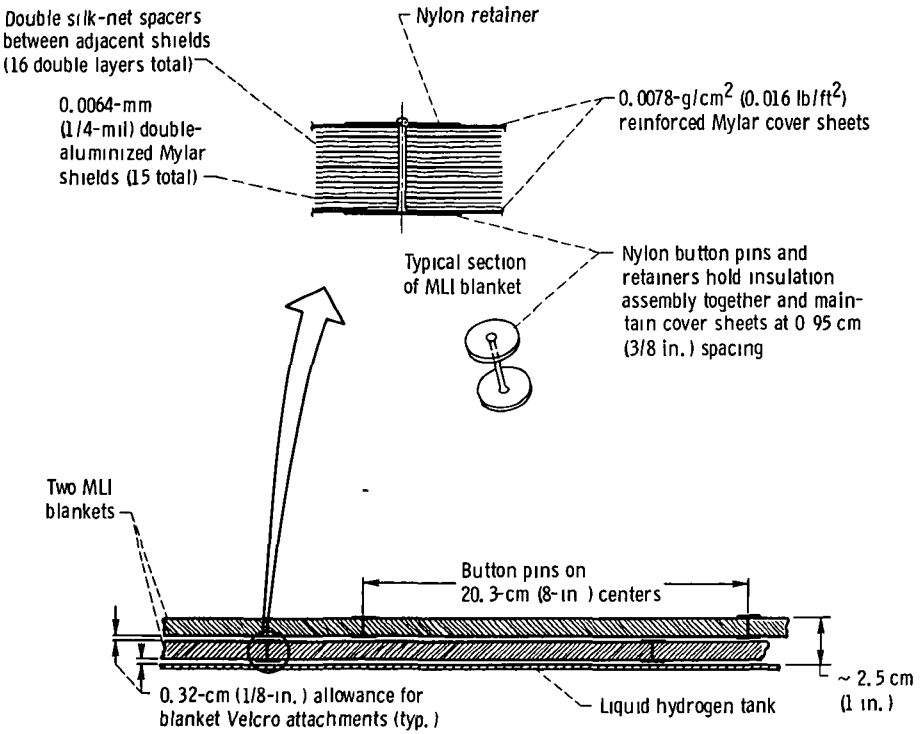

Figure 2. - Basic multilayer insulation concept. (Insulation in a helium environment during ground hold.)

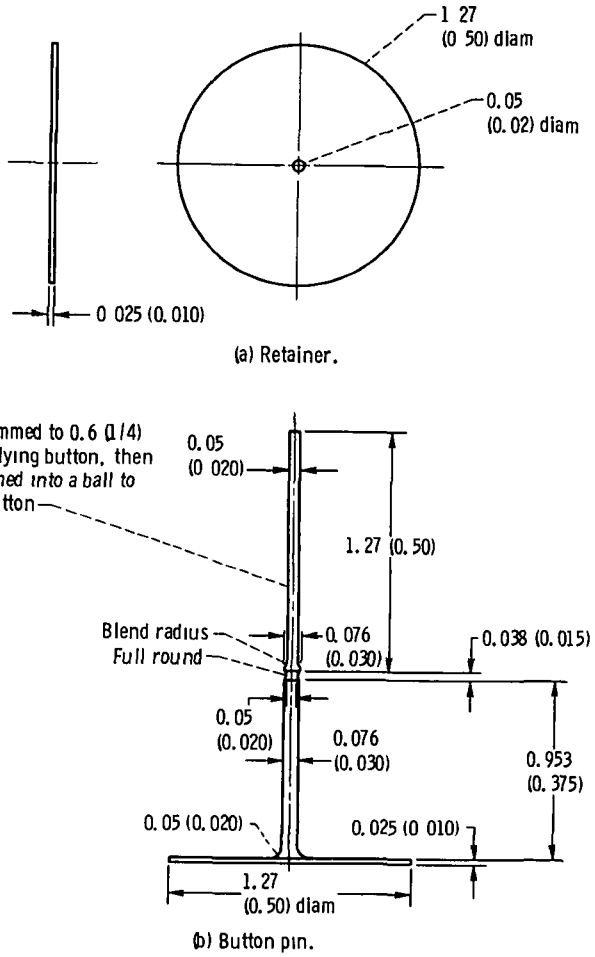

Figure 3. - Details of button pin and retainer. Material, Zytel 101 nylon resin. (All dimensions are in cm (in.).)

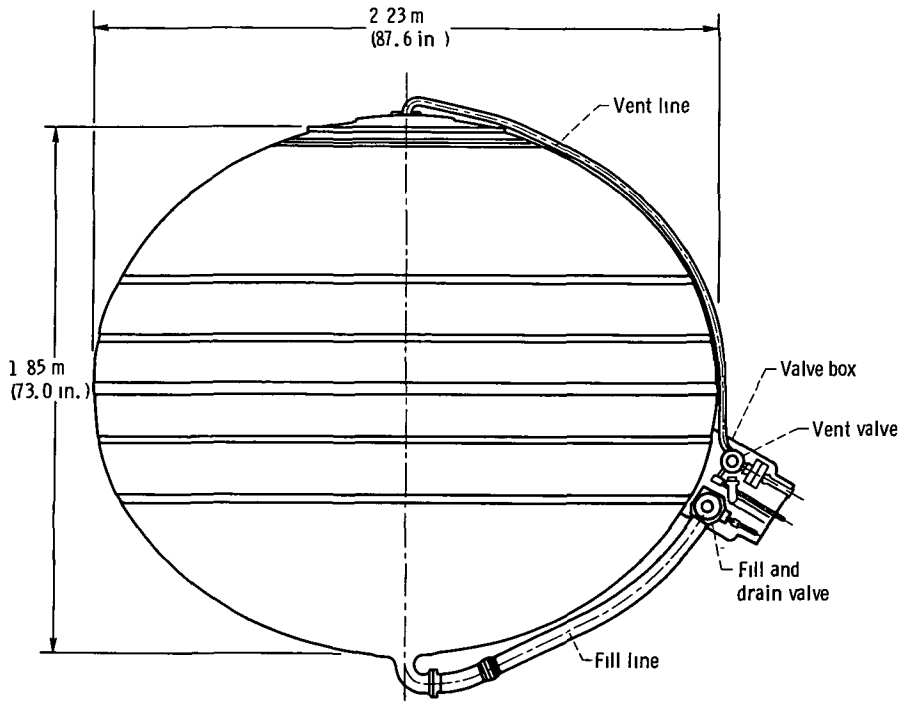

Figure 4. - Liquid hydrogen tank.

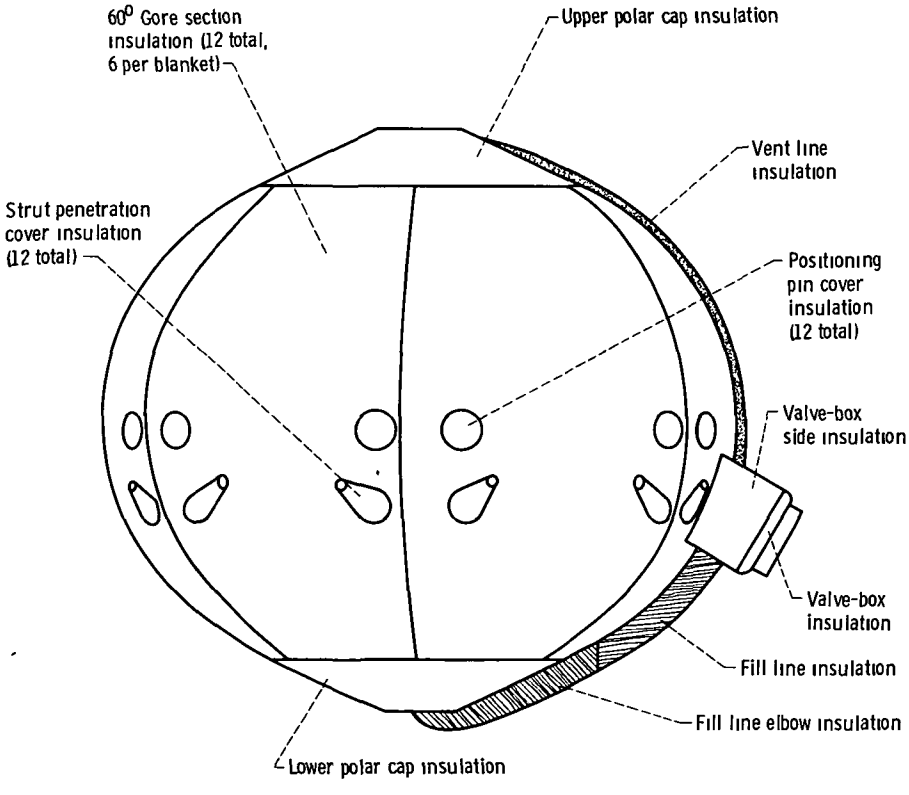

Figure 5 - Modular insulation system for liquid hydrogen tank.

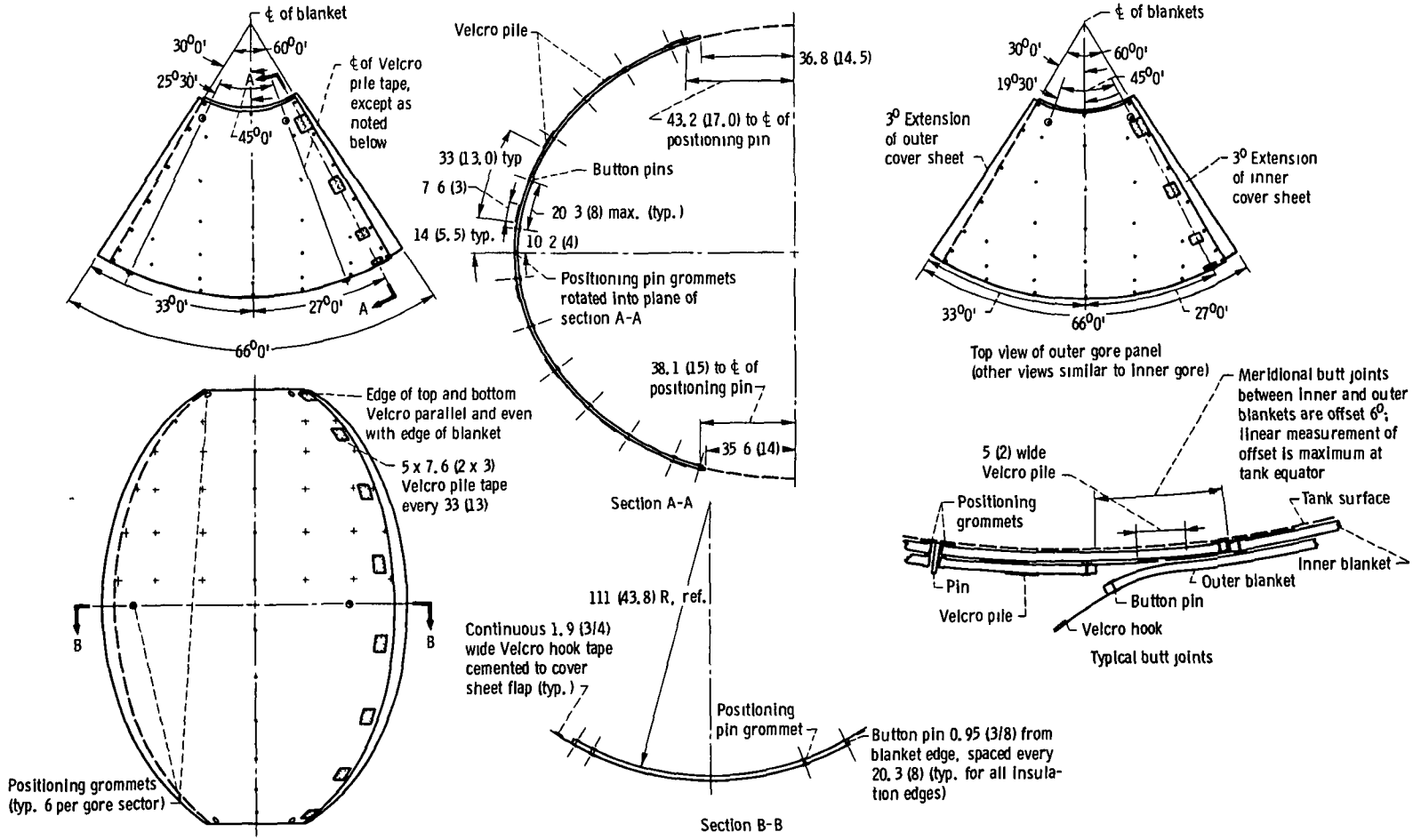

Figure 6. - Details of gore panel insulation. (All dimensions are in cm (in.) unless otherwise noted.)

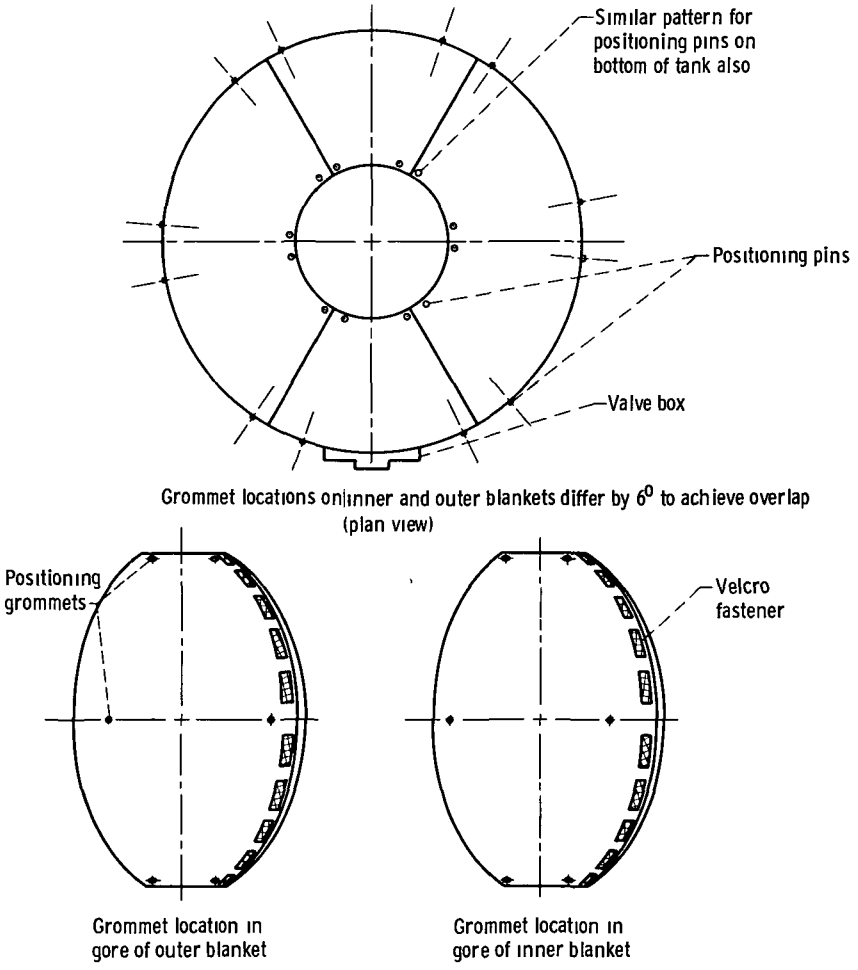

Figure 7. - Location of grommets for positioning pins.

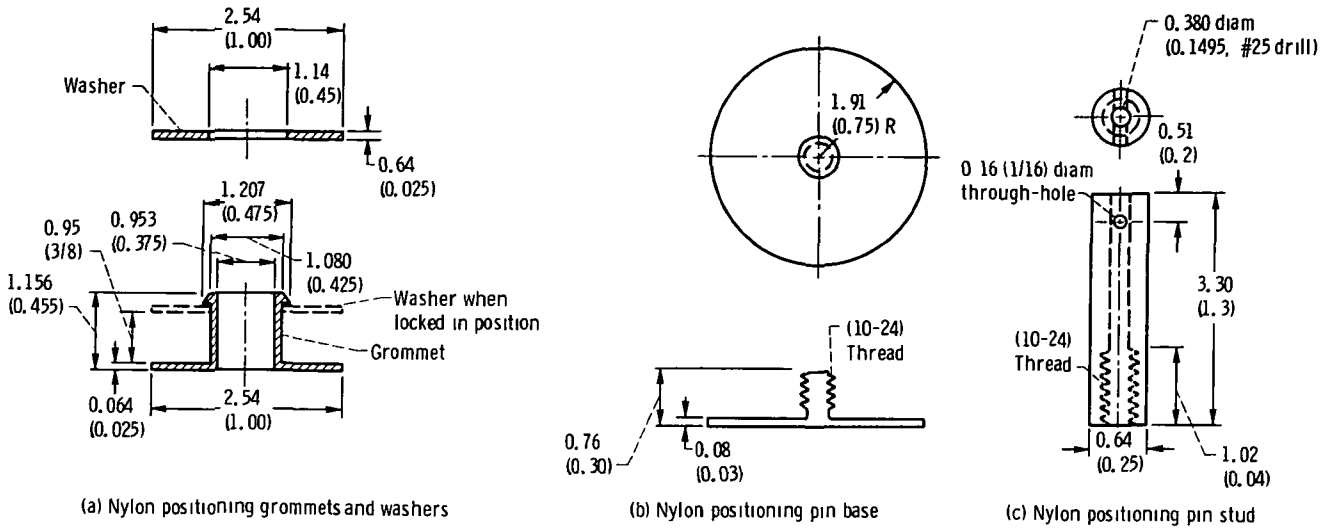

(a) Nylon positioning grommets and washers

(b) Nylon positioning pin base

(c) Nylon positioning pin stud

Figure 8. - Details of insulation positioning pin. (All dimensions are in cm (in.) unless otherwise noted.)

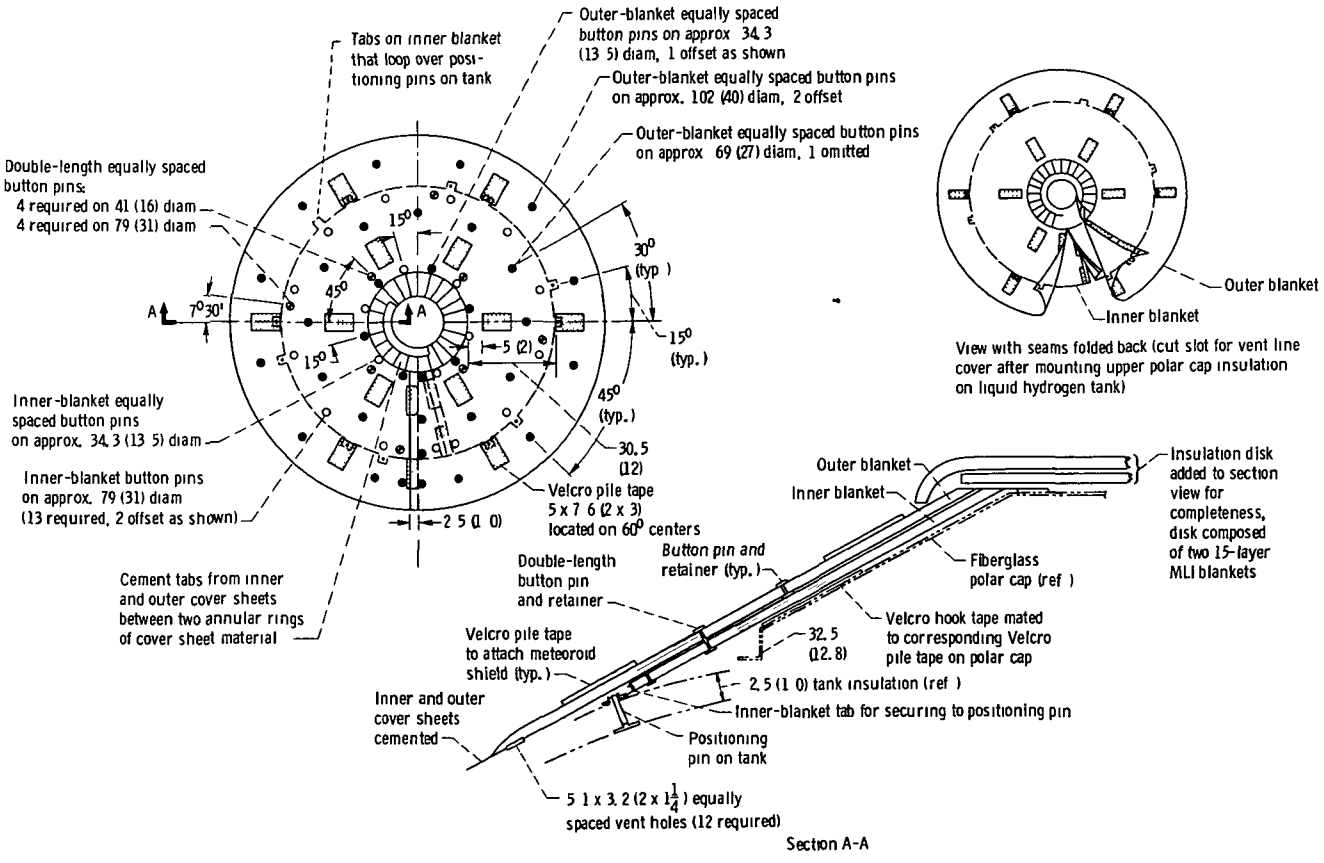

Figure 9 - Details of upper polar cap insulation (All dimensions are in cm (in.) unless otherwise noted.)

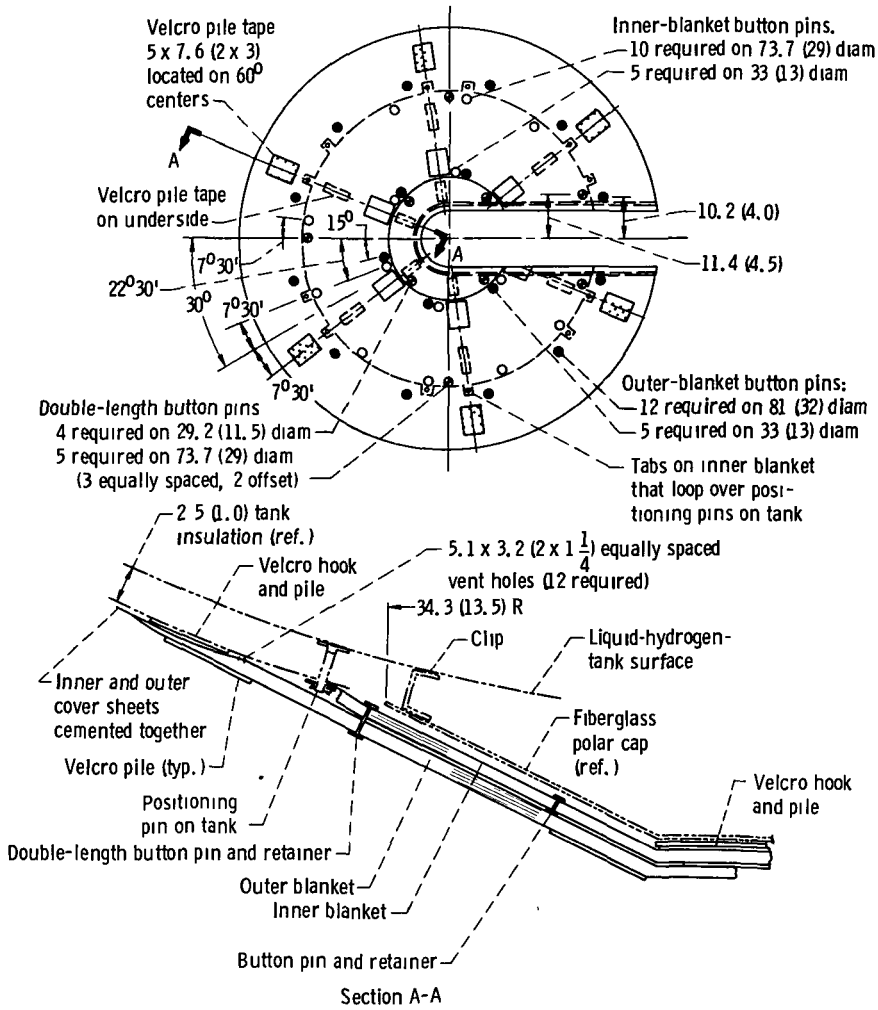

Figure 10. - Lower polar cap insulation. (All dimensions are in cm (in.) unless noted otherwise.)

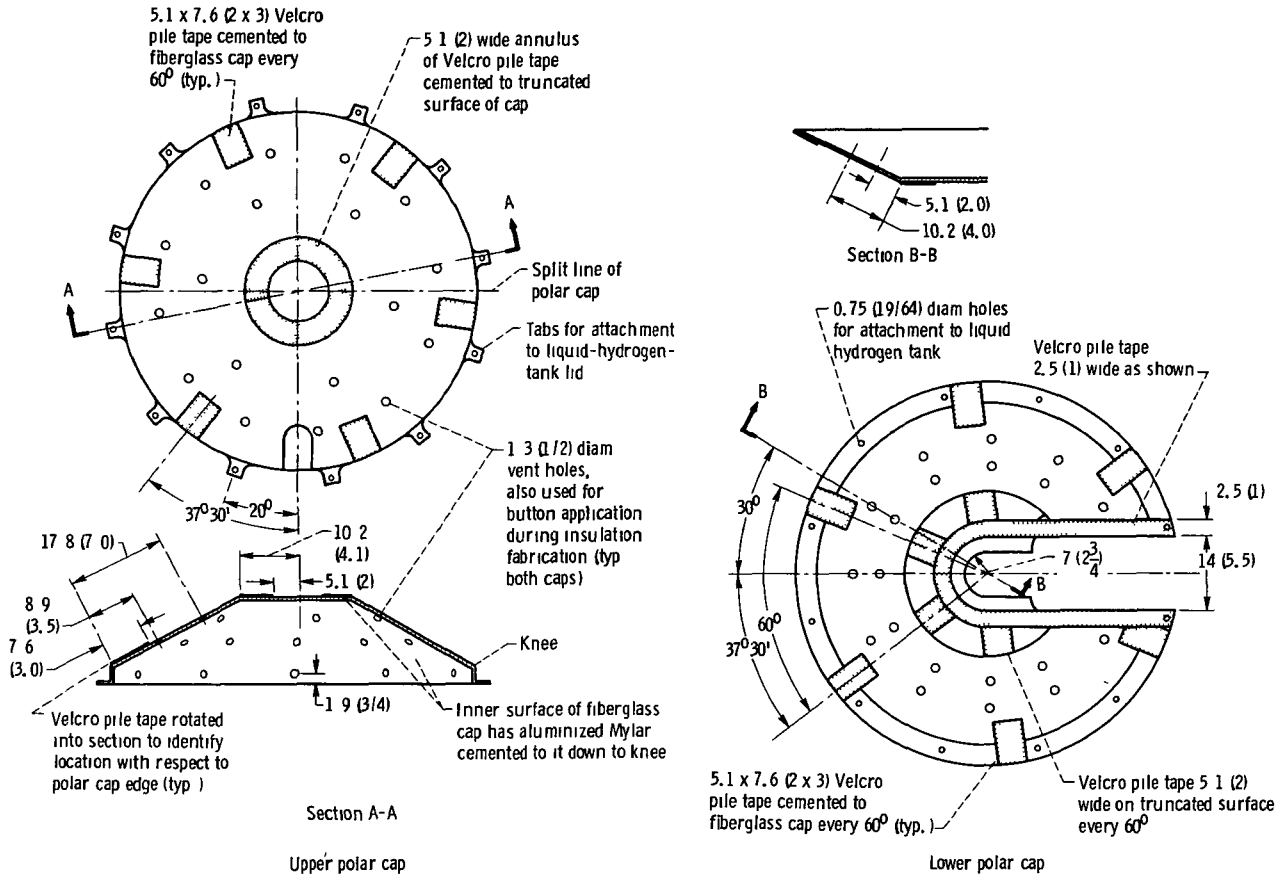

Figure 11 - Upper and lower fiberglass polar caps (Velco-pile tape mates with Velcro hook tape attached to insulation, see figs. 9 and 10. All dimensions are in cm (in.) unless noted otherwise.)

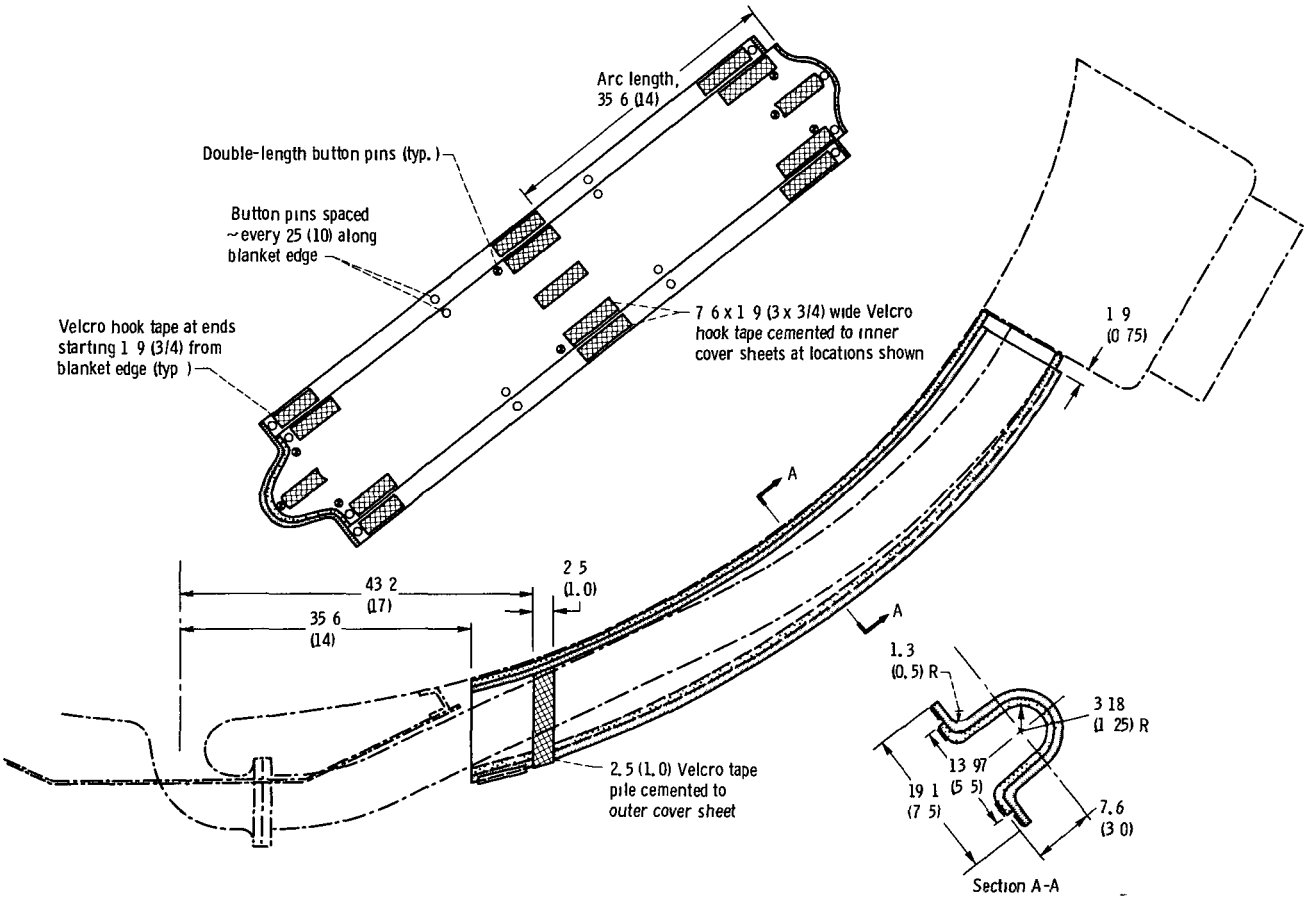

Figure 12. - Fill line insulation cover for liquid hydrogen tank (All dimensions are in cm (in) unless noted otherwise

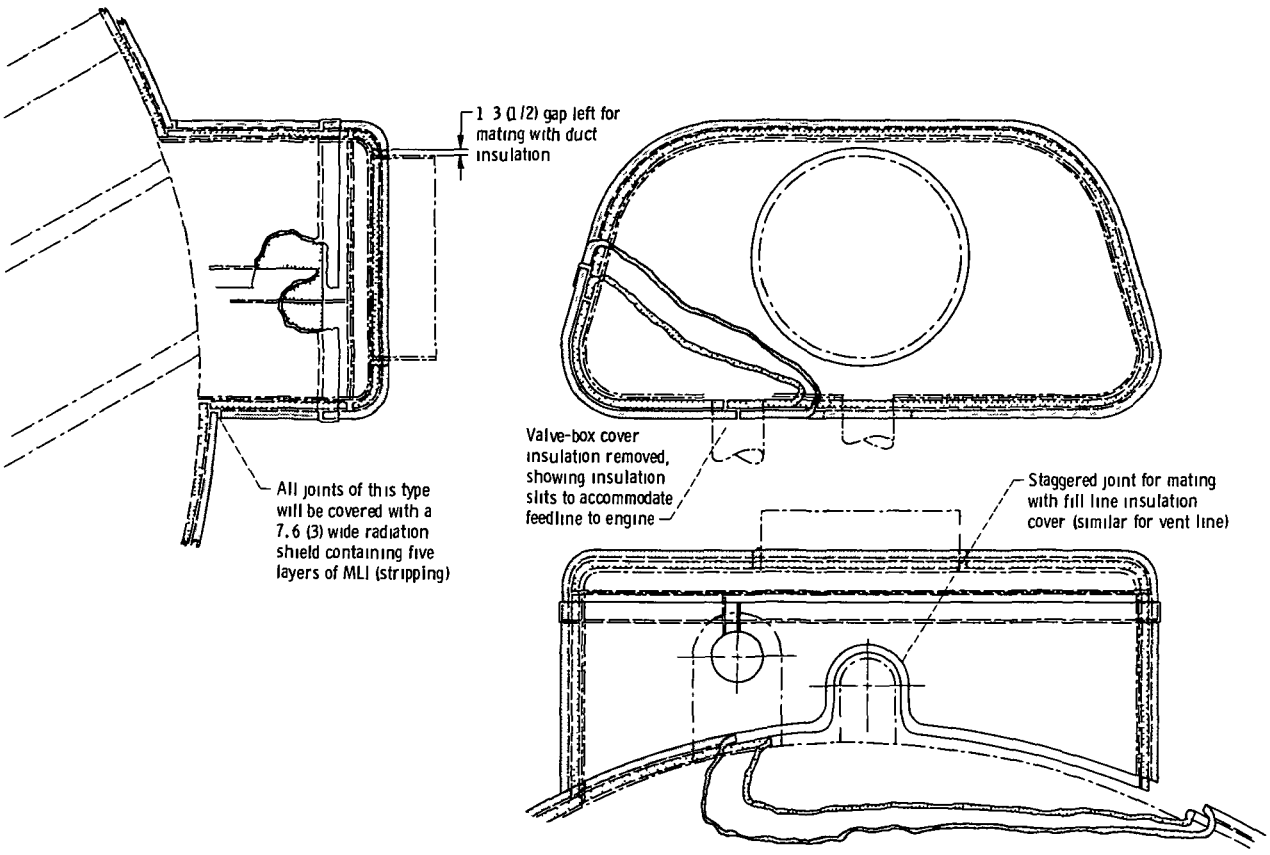

Figure 13. - Valve-box insulation. (All dimensions are in cm (in.) unless noted otherwise)

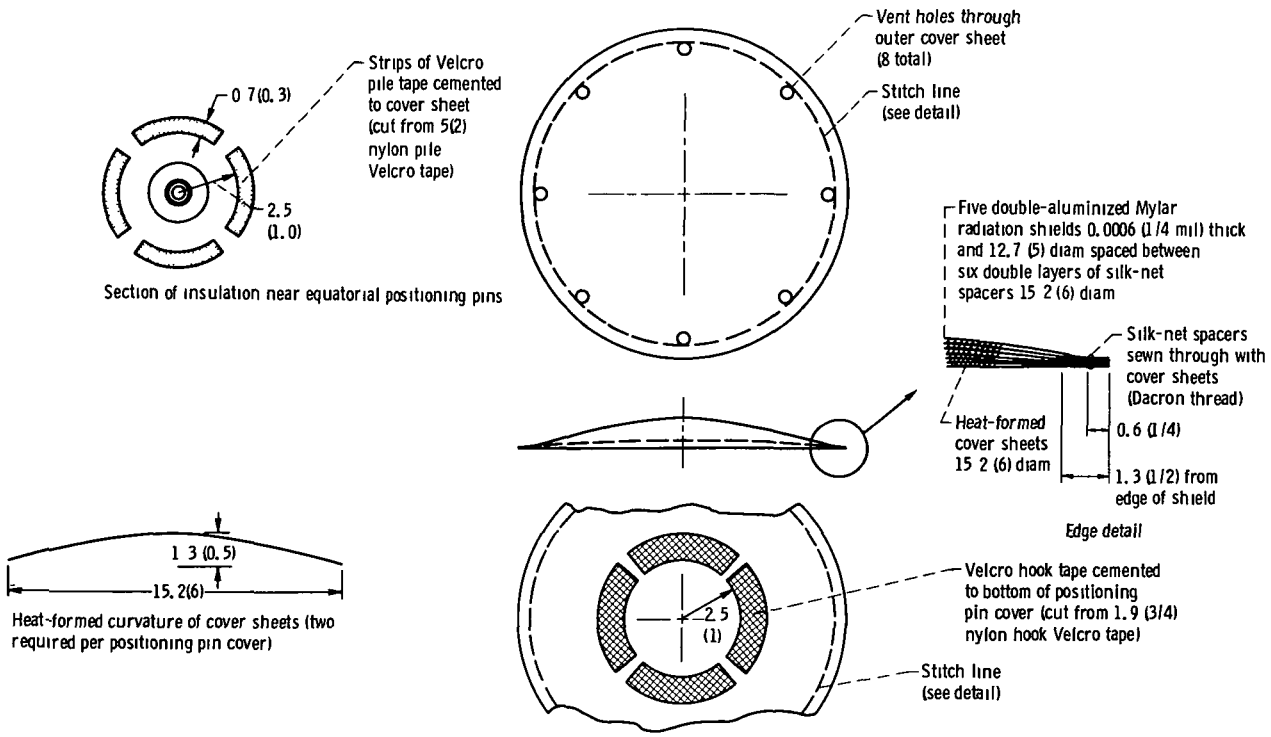

(a) Positioning pin cover.

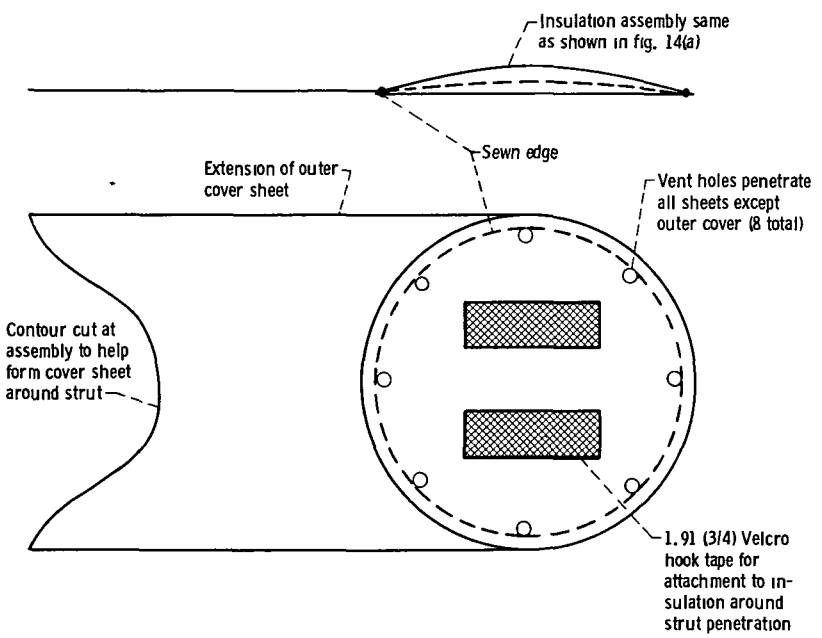

(b) Strut penetration cover

Figure 14 - Insulation covers. (All dimensions are in cm (in.) unless noted otherwise)

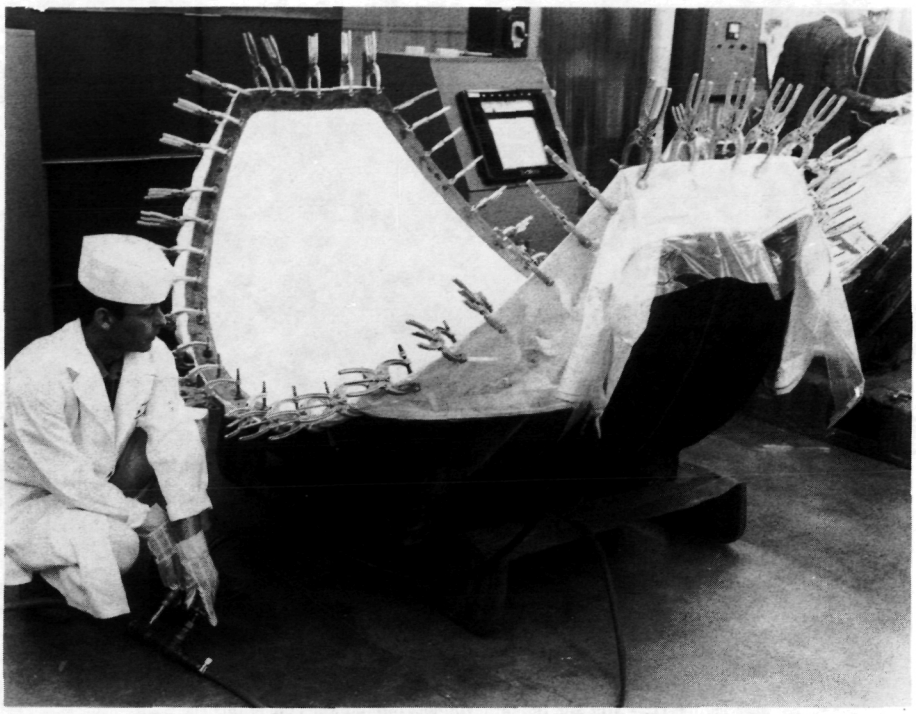

Figure 15. - Thermovacuum forming of gore panel radiation shields (17 layers.)

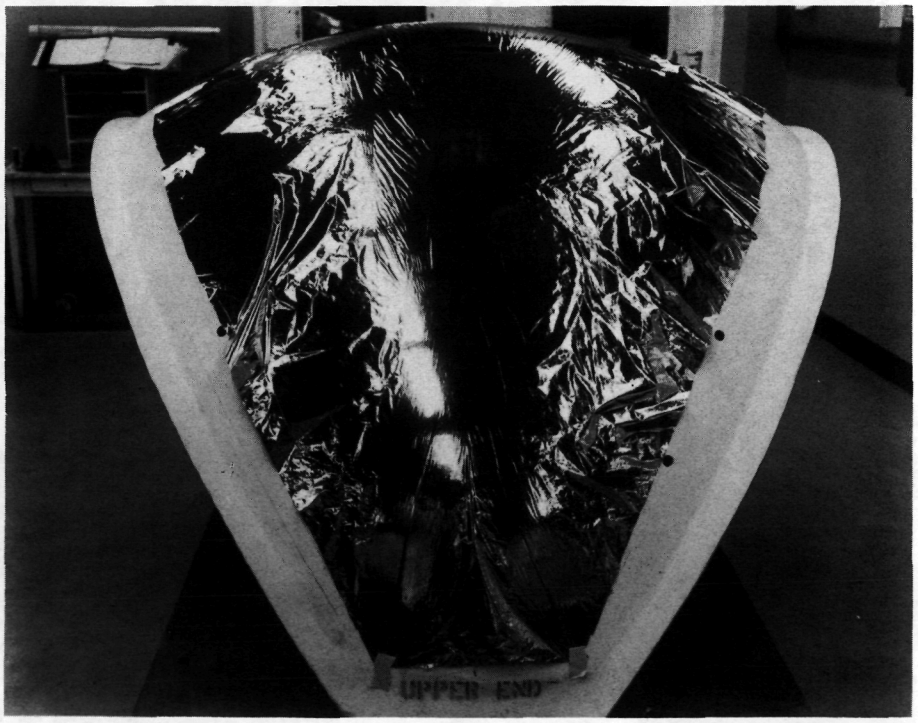

Figure 16. - Layup of single sheet of double-aluminized Mylar to demonstrate degree of forming achieved.

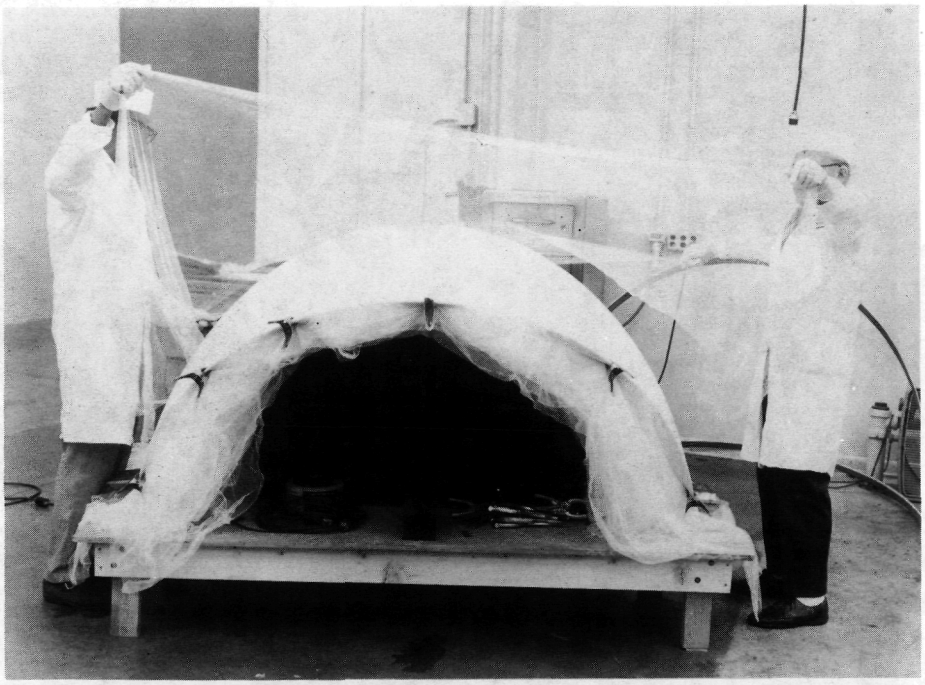

Figure 17. - Wet silk net on layup tool during water forming process.

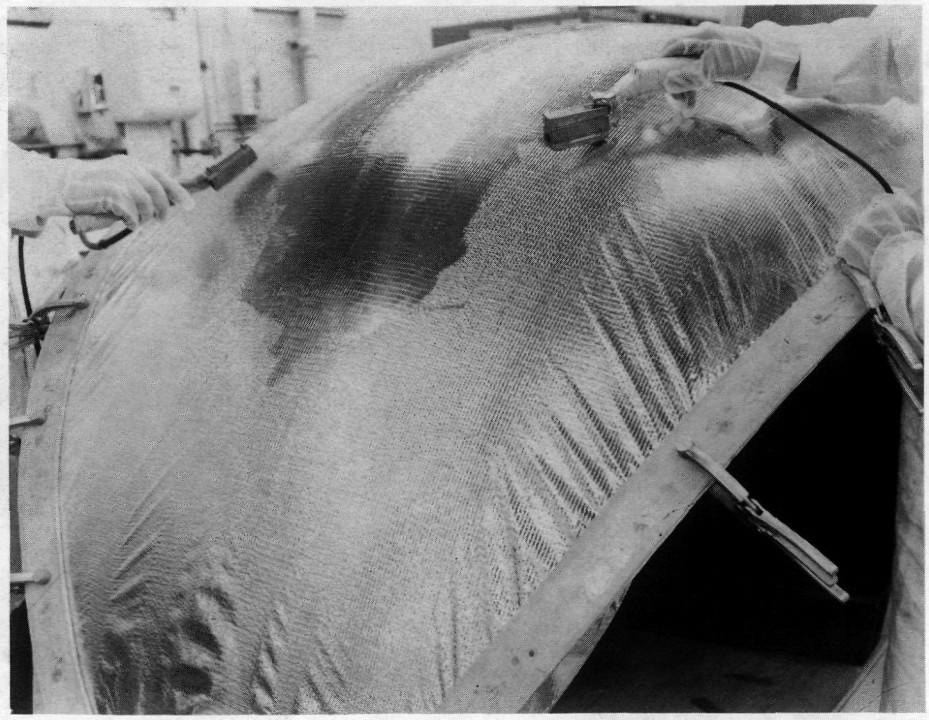

Figure 18. - Hand ironing of partially formed reinforced-Mylar cover sheet on layup tool.

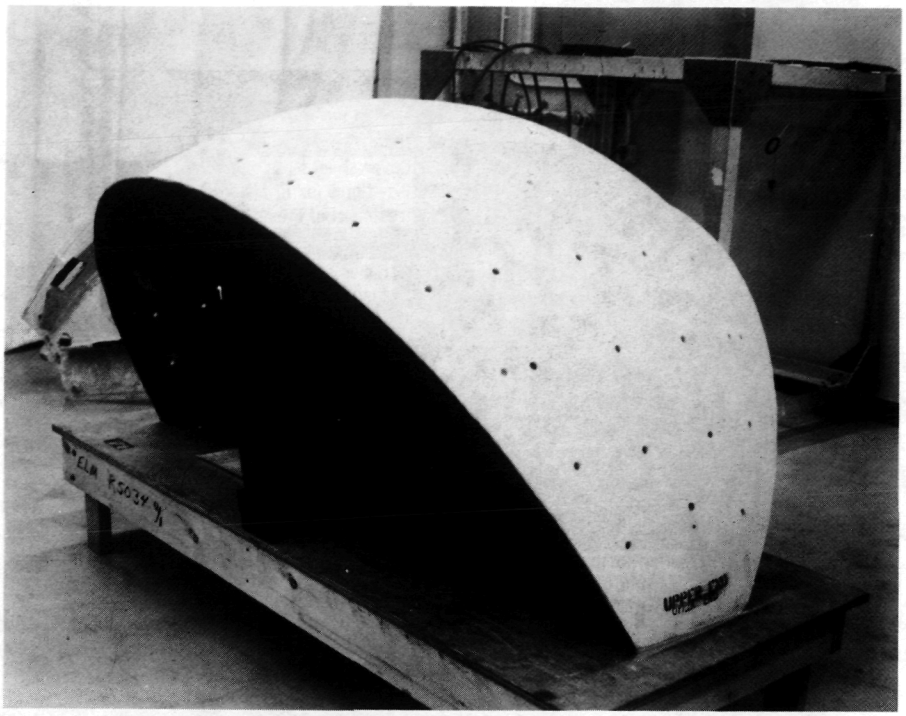

(a) Gore panel layup tool.

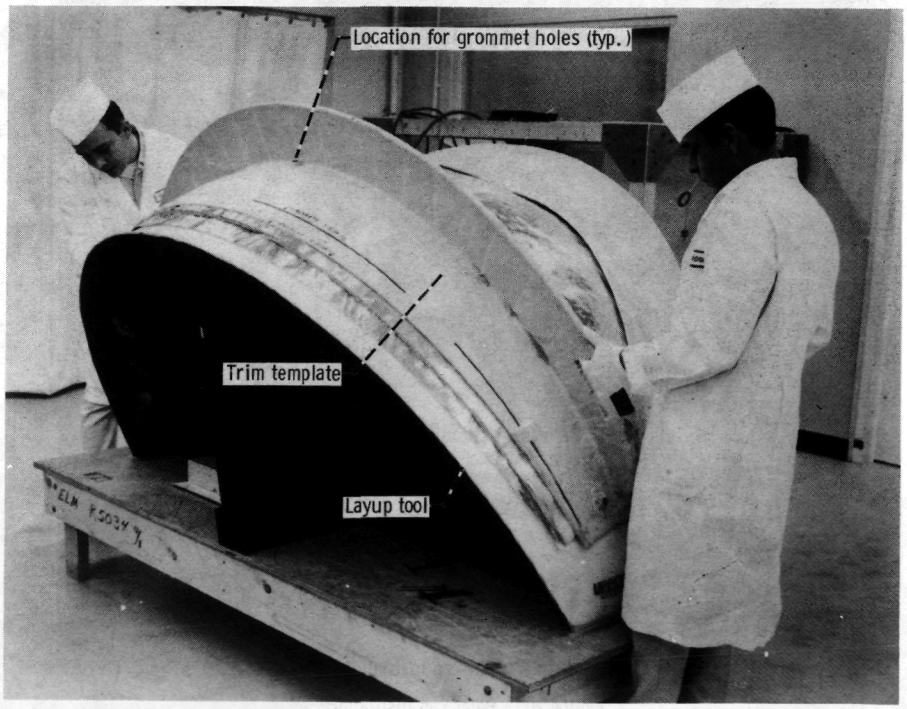

(b) Trim template applied to gore panel insulation.

Figure 19. - Gore-section layup and trimming hardware.

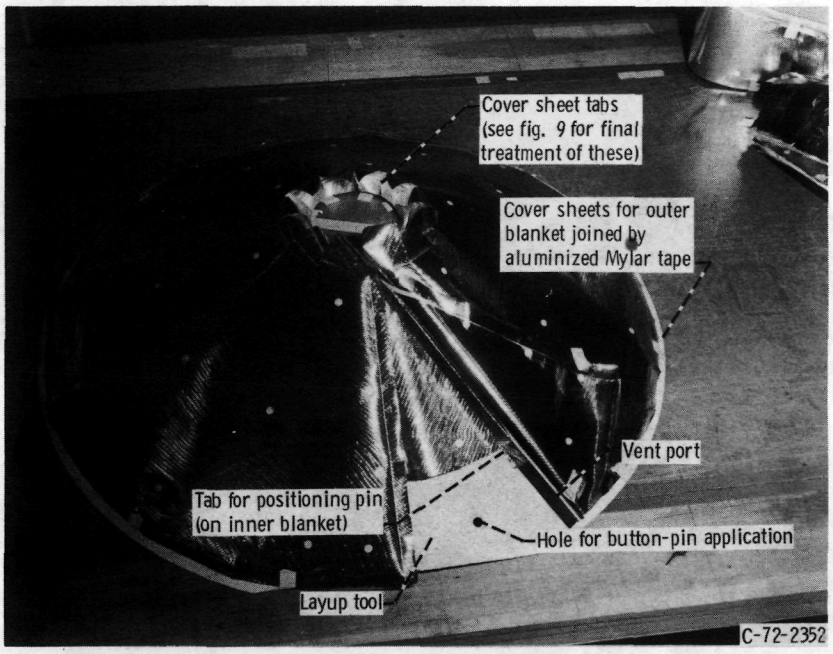

(a) Upper polar cap insulation.

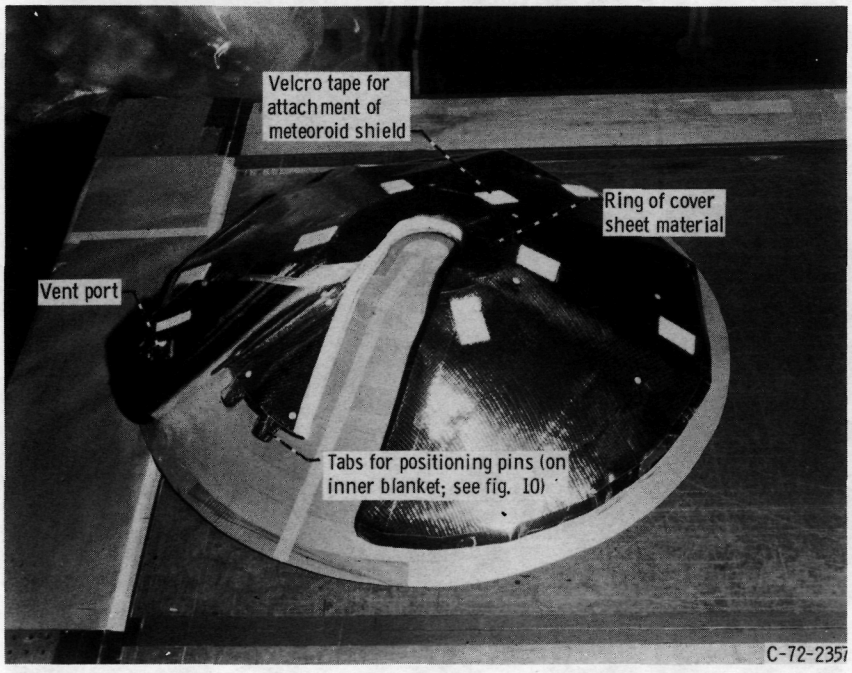

(b) Lower polar cap insulation.

Figure 20. - Polar cap insulation.

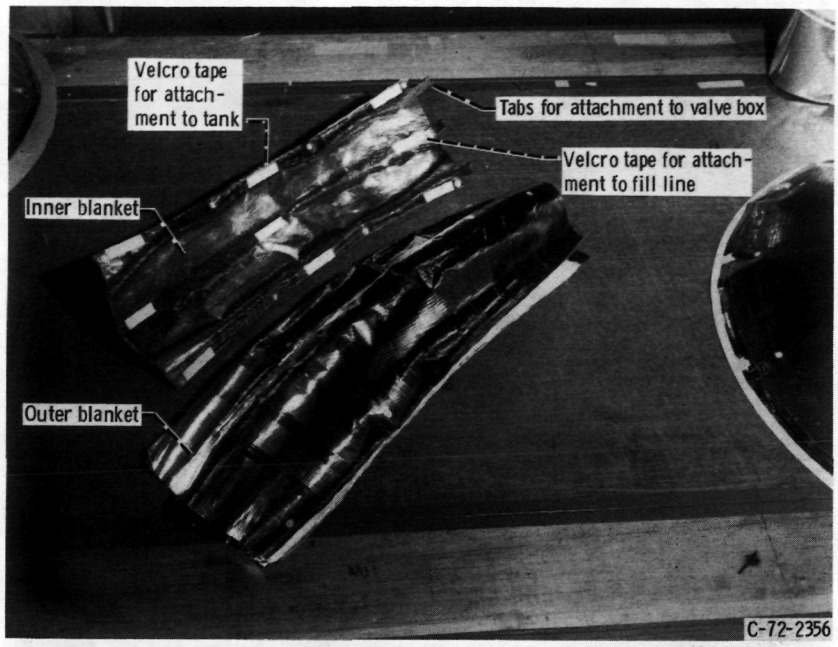

(a) Fill line insulation.

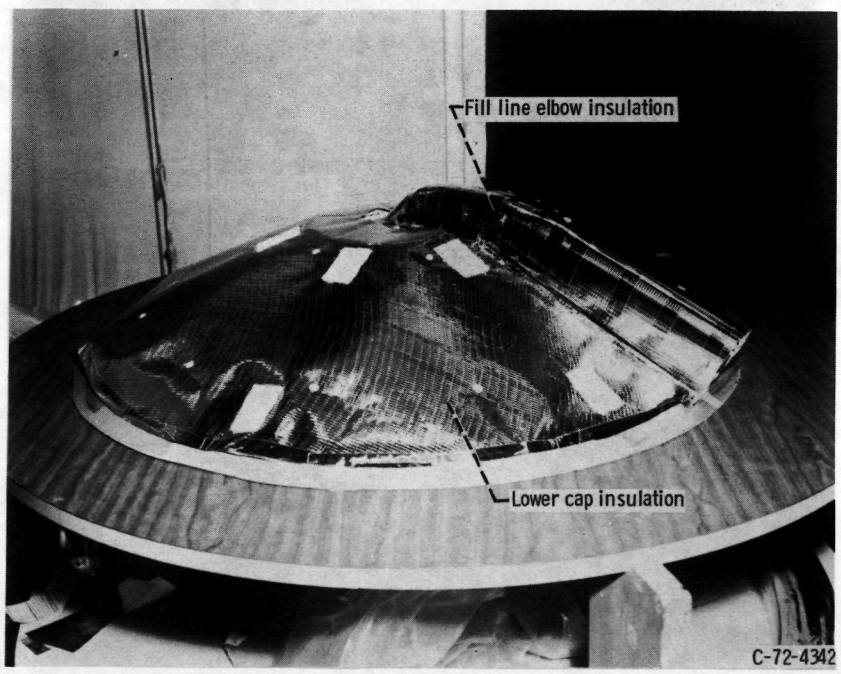

(b) Fill line elbow insulation mated with lower cap insulation.

Figure 21. - Tank lower-line insulation.

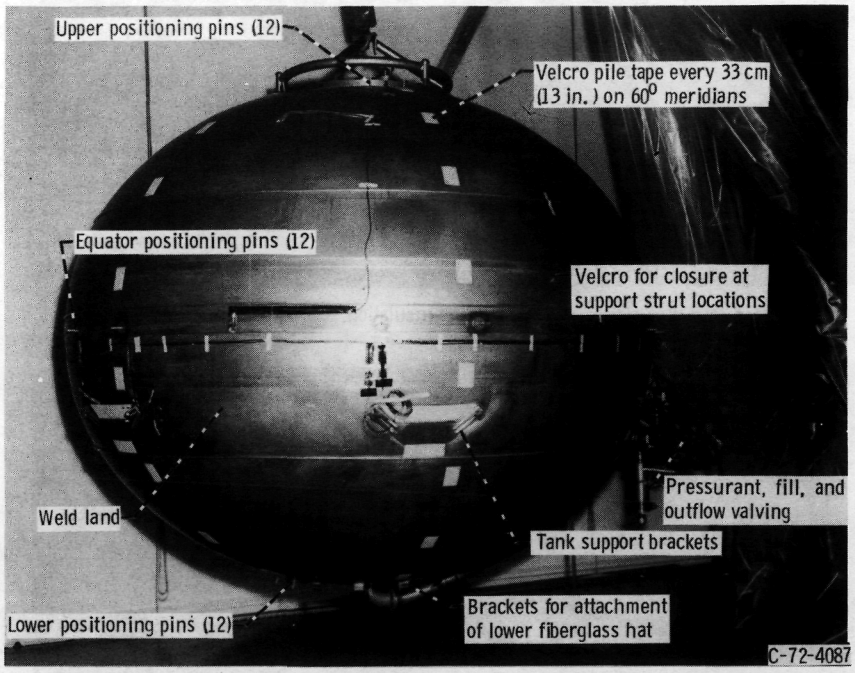

Figure 22. - Hydrogen tank with positioning pins and Velcro tape applied.

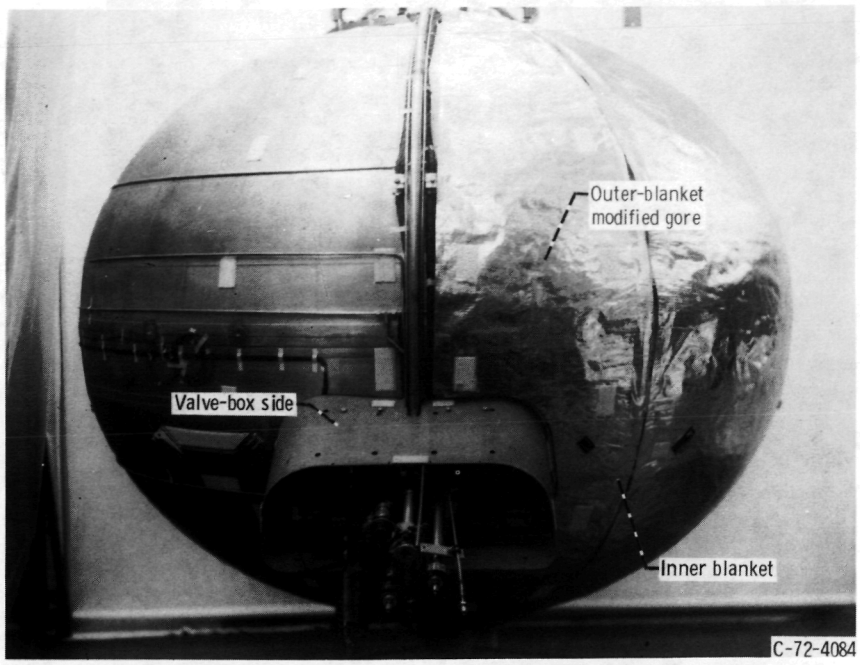

(a) Modification of MLI gore at valve box.

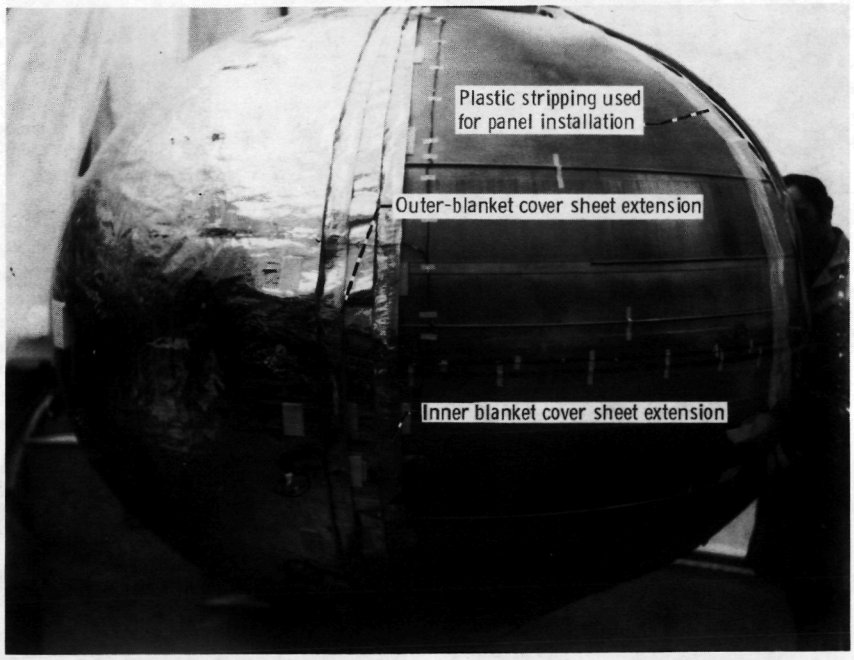

(b) Exposed seams of both blankets.

Figure 23. - Application of gore panels.

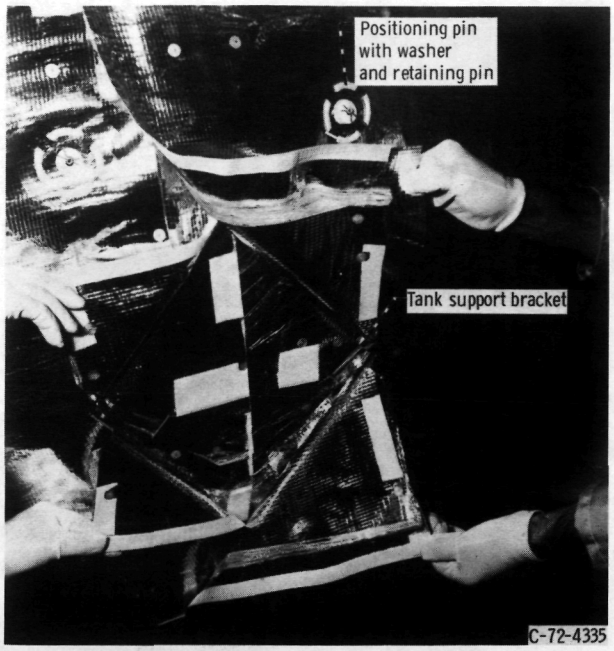

(c) Detail at tank support area.

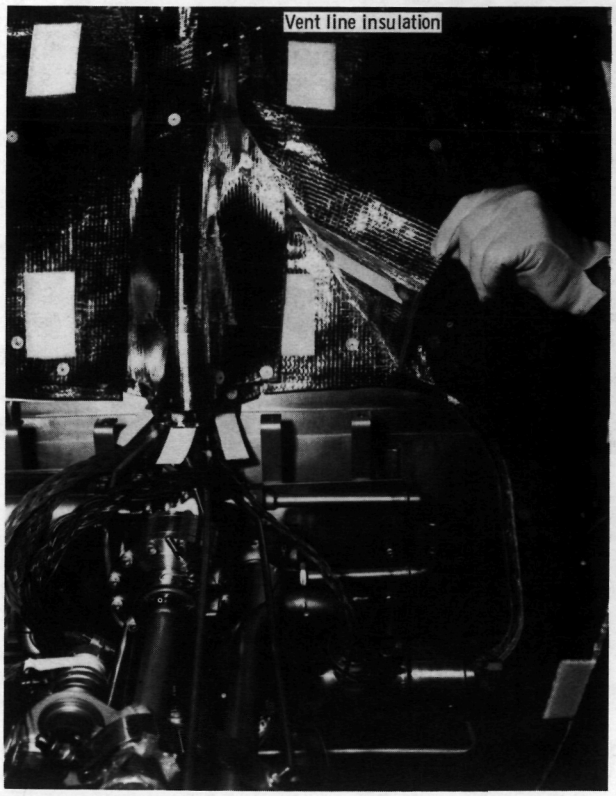

(d) Detail of vent line insulation near valve-box area.

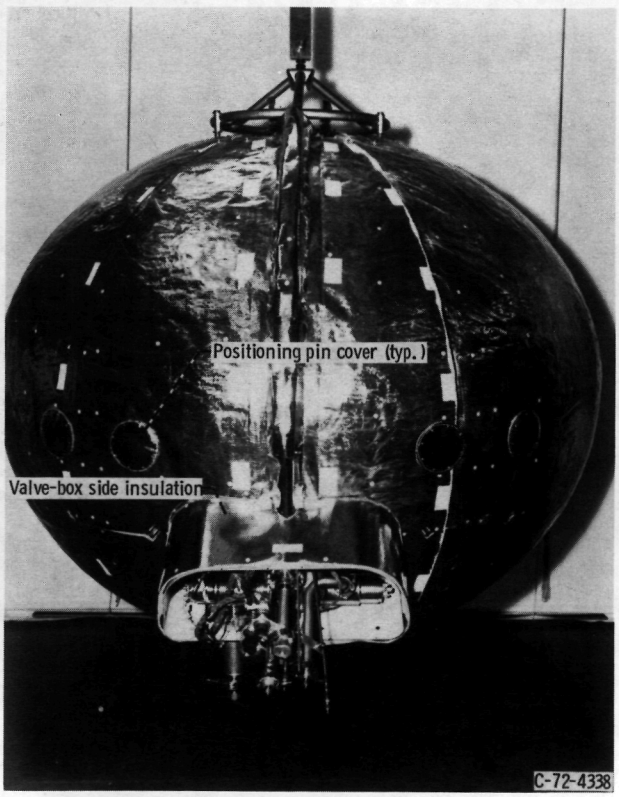

(e) All gore panels applied.

Figure 23. - Concluded.

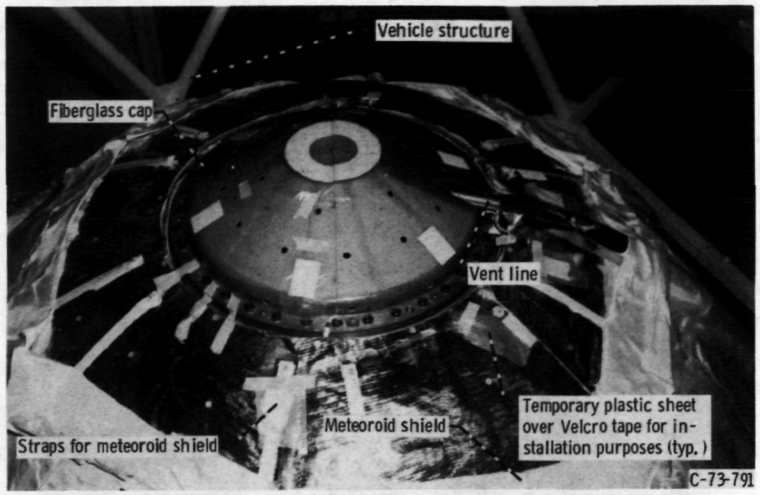

(a) Fiberglass cap in place.

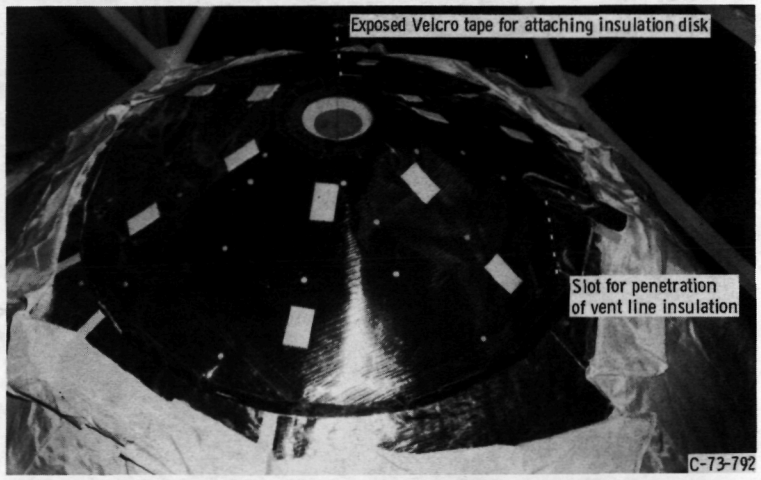

(b) Cap insulation applied.

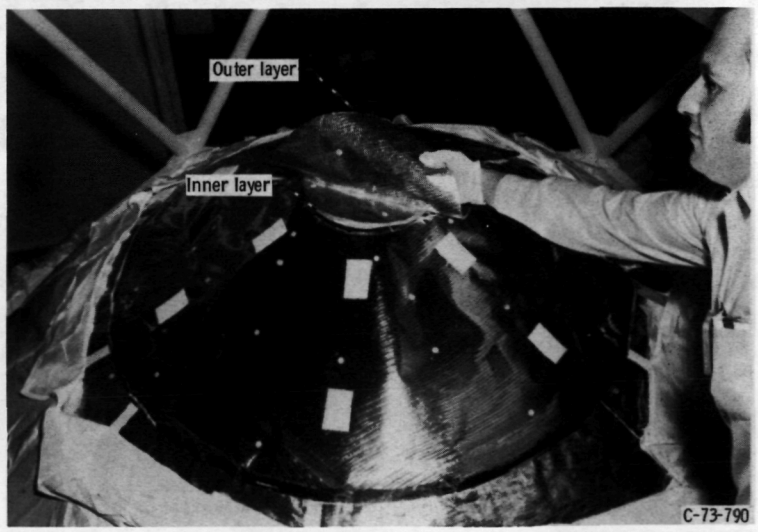

(c) Adding insulation disk.

Figure 24. - Application of upper polar cap insulation.

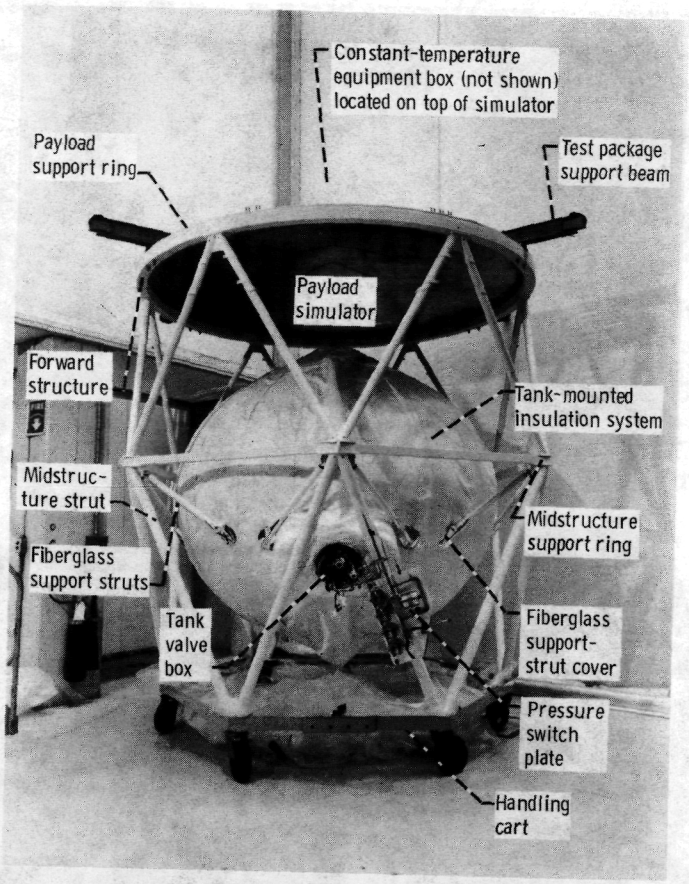

Figure 25. - Insulated-tank test package.

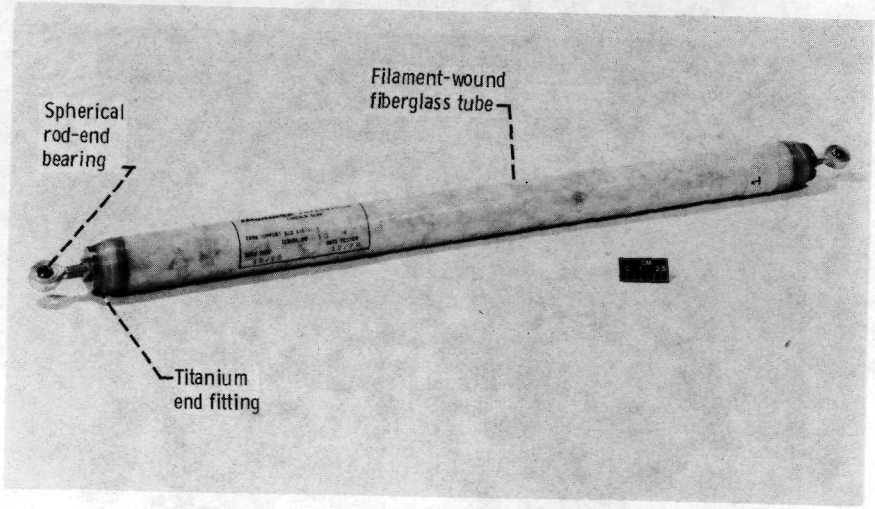

Figure 26. - Liquid-hydrogen-tank fiberglass support strut.

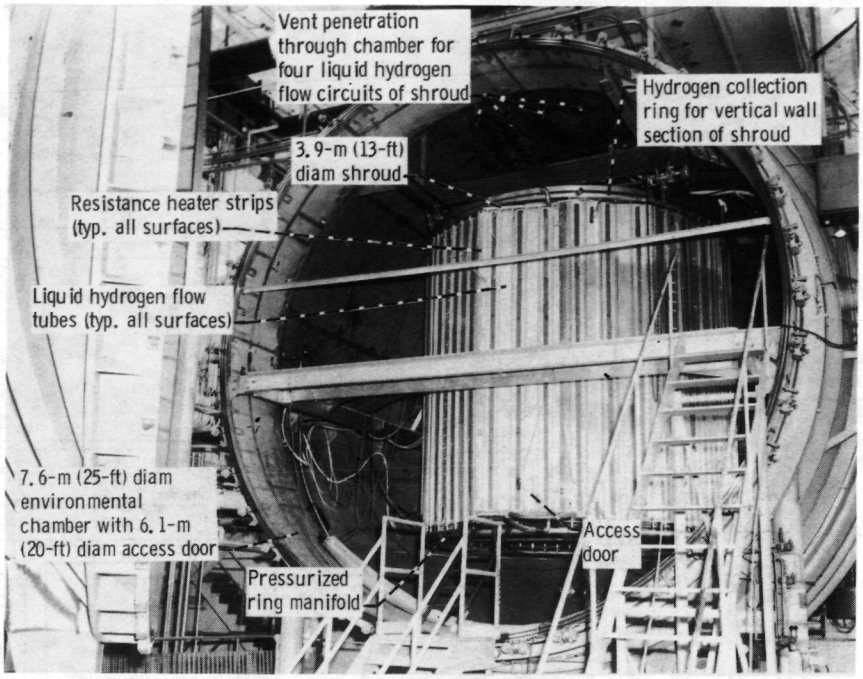

Figure 27. - Shroud positioned in vacuum chamber.

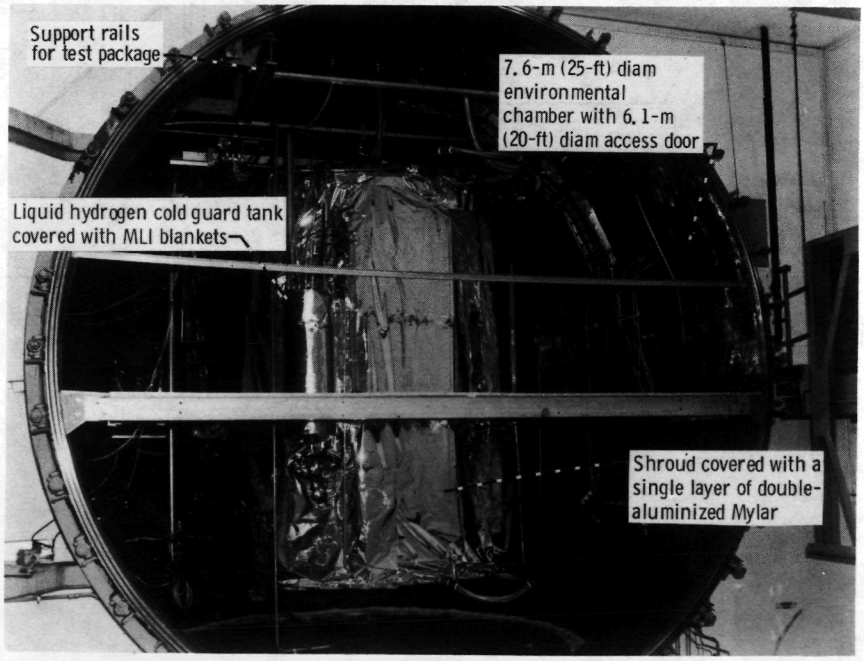

Figure 28. - Liquid hydrogen cold guard tank mounted on shroud.

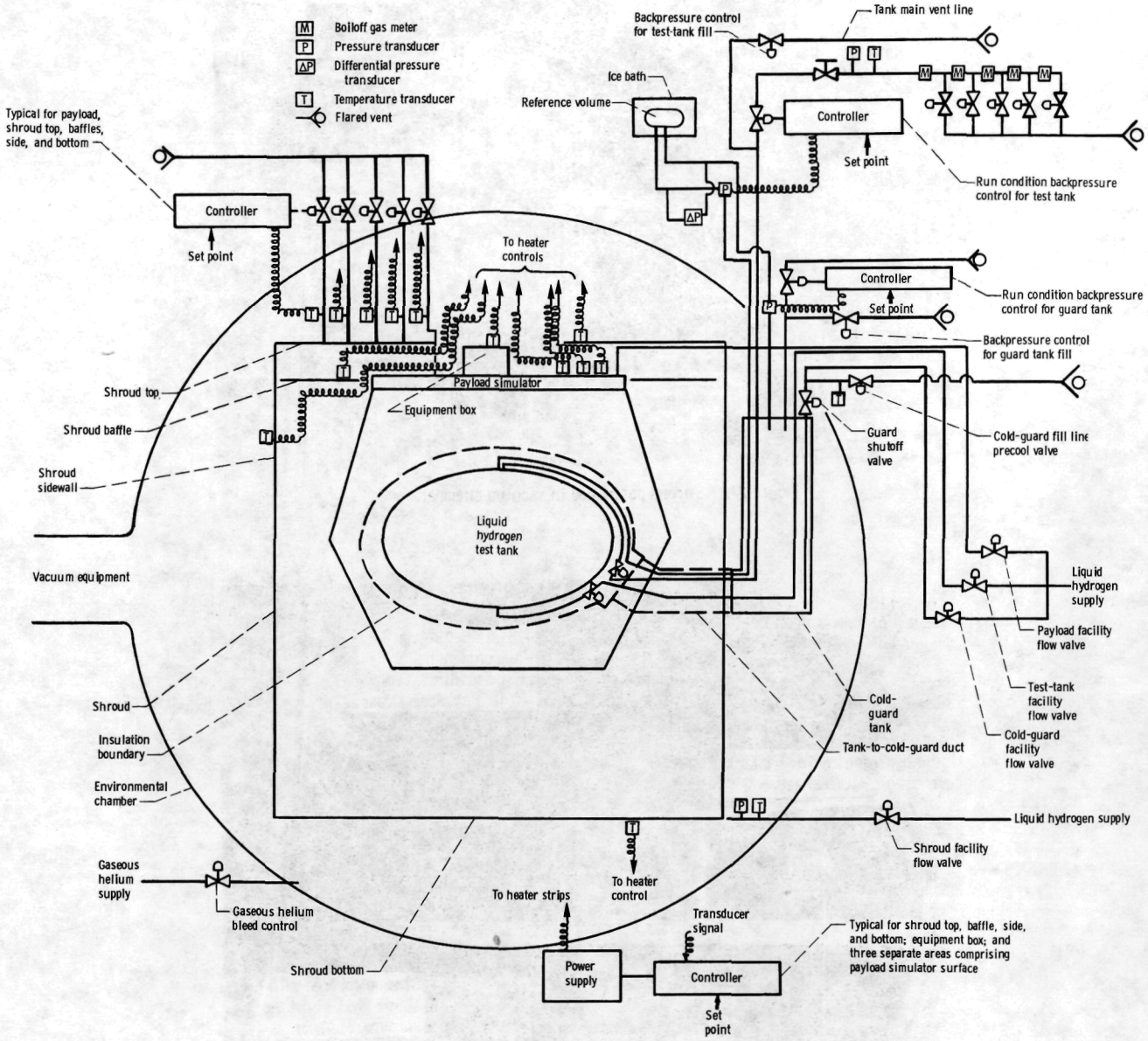

Figure 29. - Facility plumbing and control circuits.

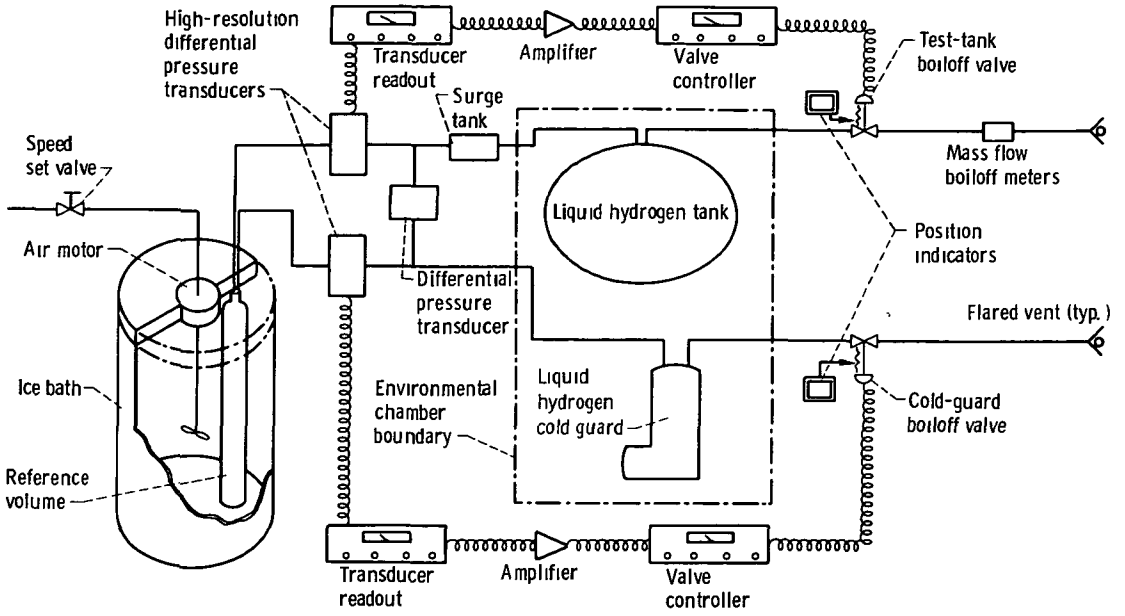

Figure 30. - Block diagram of test-tank and cold-guard backpressure control systems

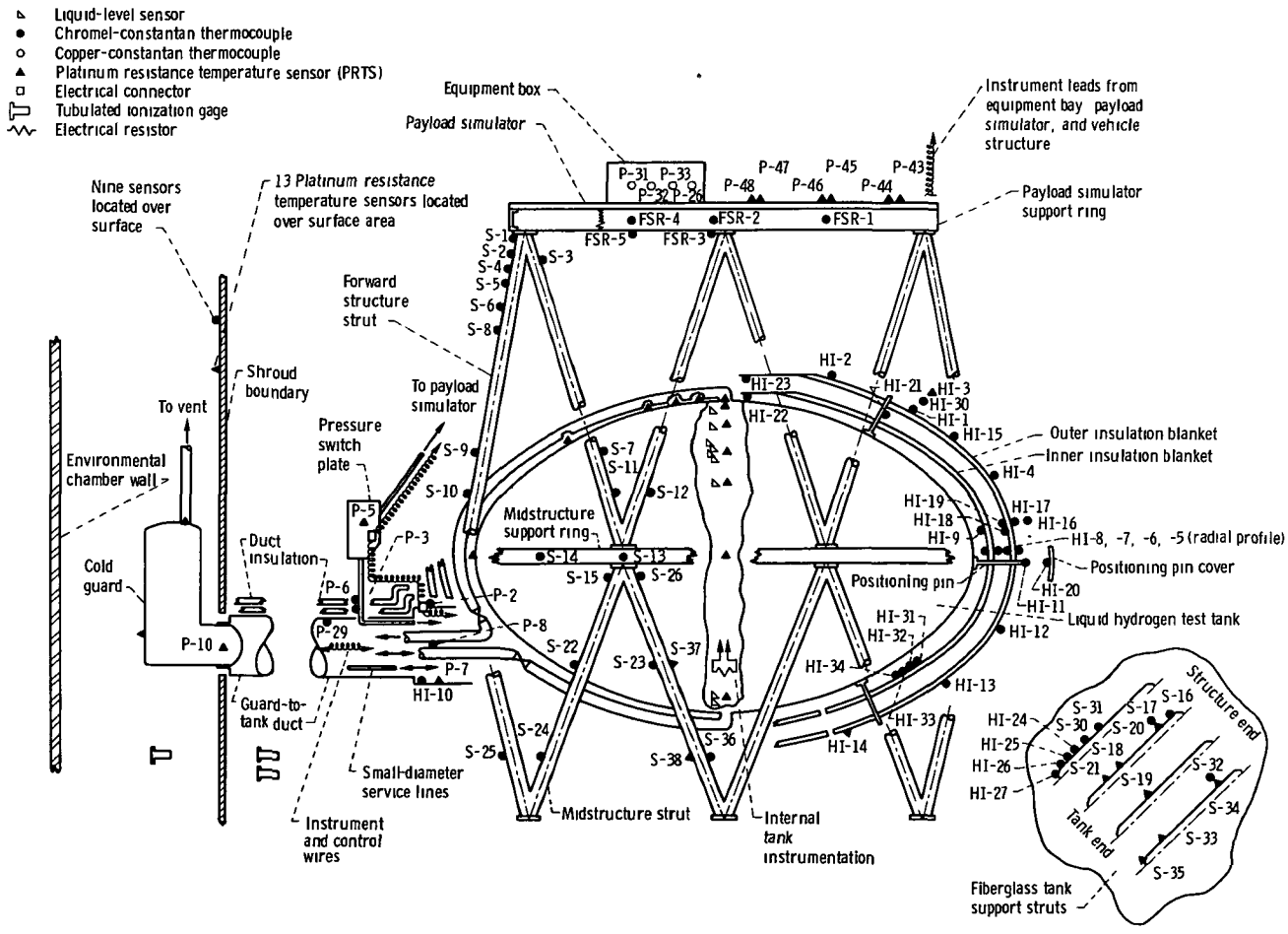

Figure 31. - Instrumentation

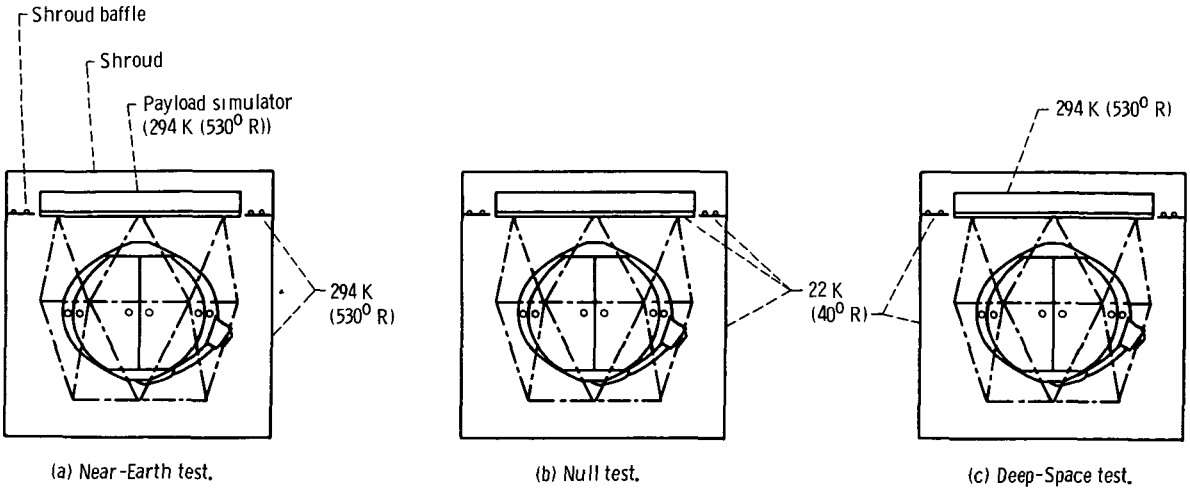

Figure 32. - Sketch of test-tank environmental surroundings for Near-Earth, Null, and Deep-Space tests.

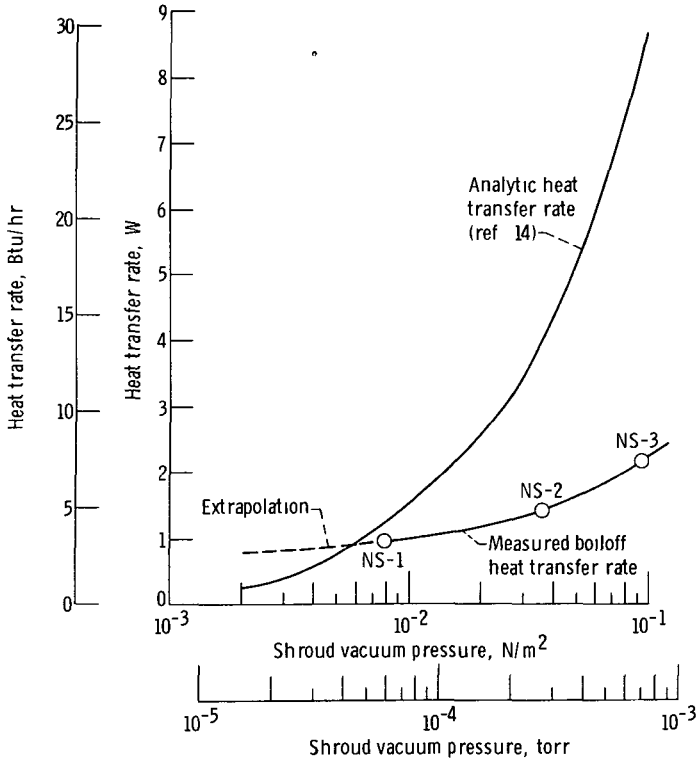

Figure 33 - Deep-space-simulation heat transfer rate as function of shroud vacuum pressure

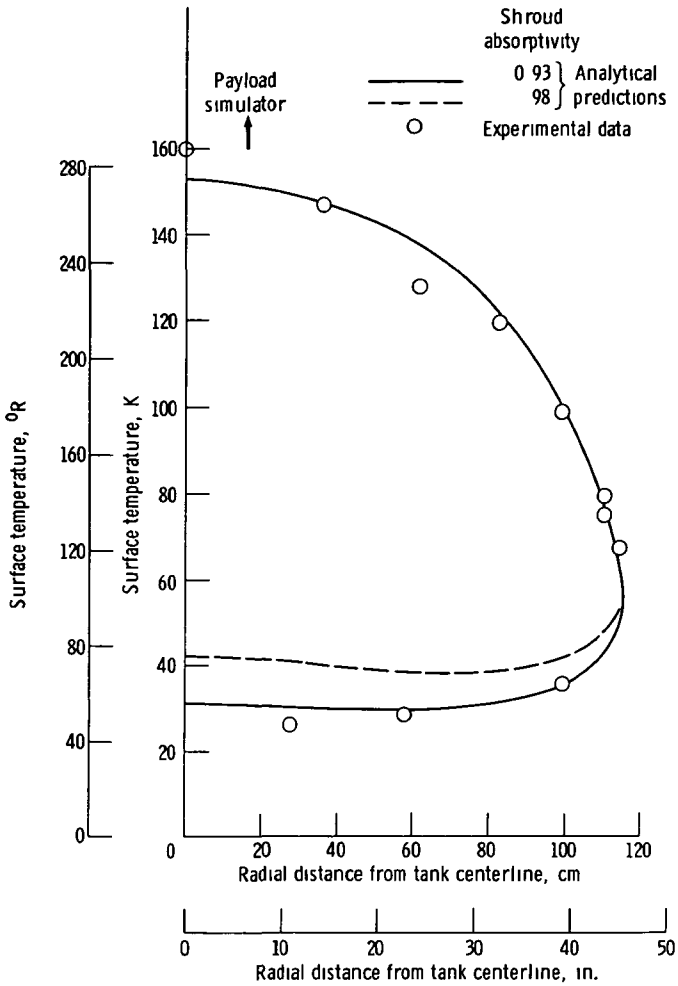

Figure 34. - Temperature profile of insulation surface for deep-space simulation. Payload temperature, 287 K (516° R), shroud temperature, 23 3 K (42° R)

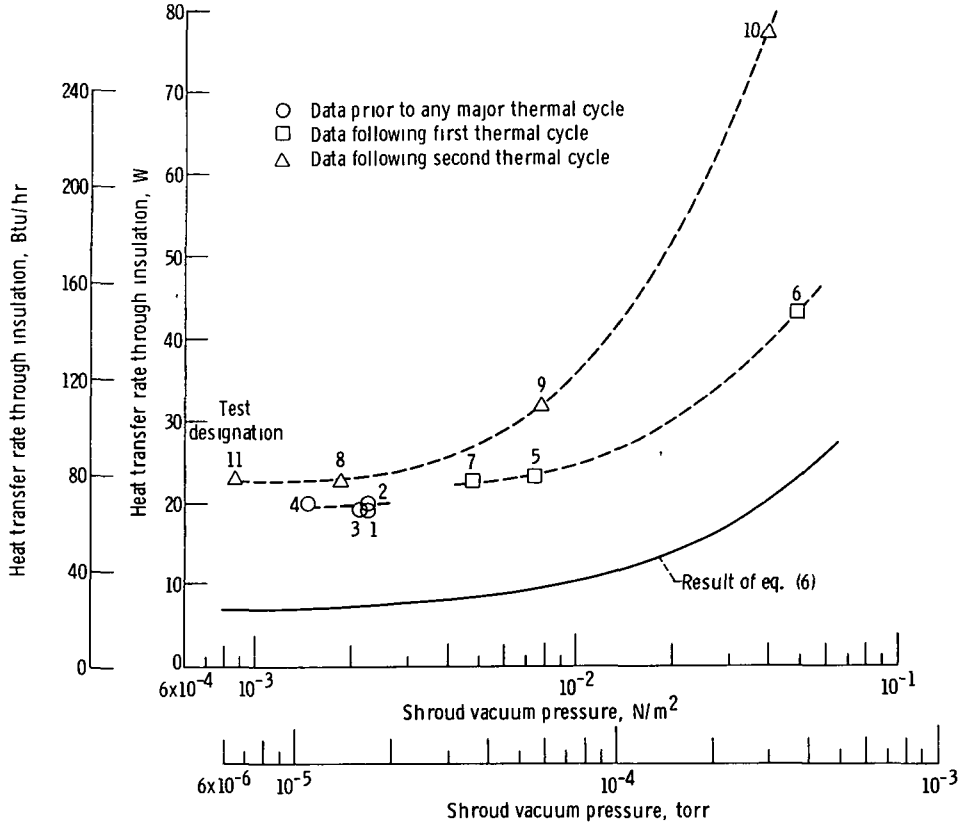

Figure 35 - Heat transfer rate through insulation as function of shroud vacuum pressure level

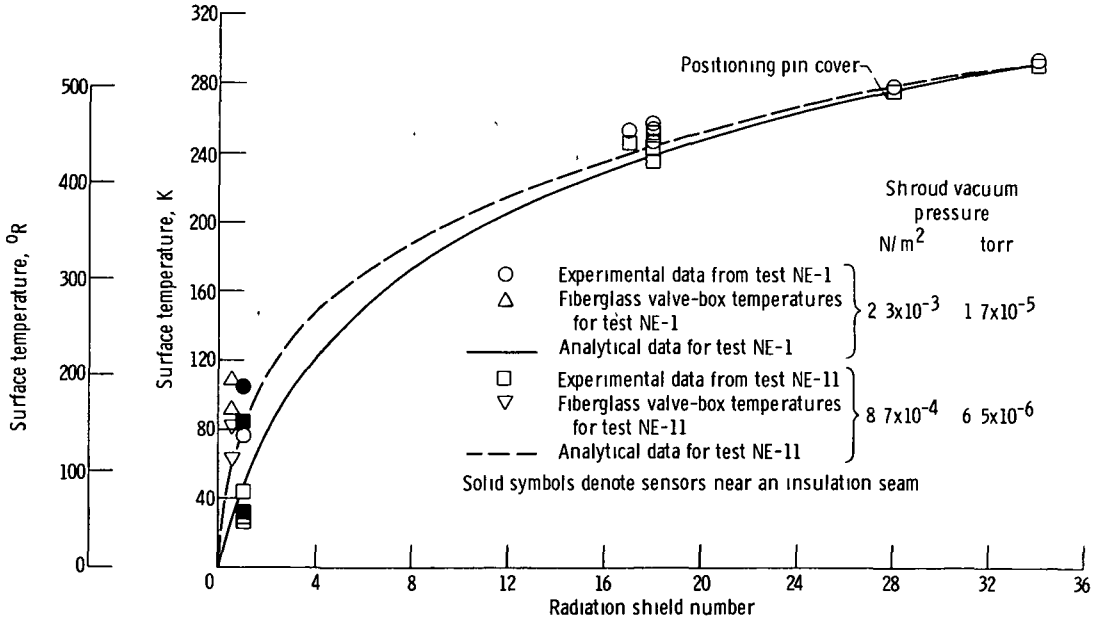

Figure 36 - Temperature profile of insulation surface for selected Near-Earth tests

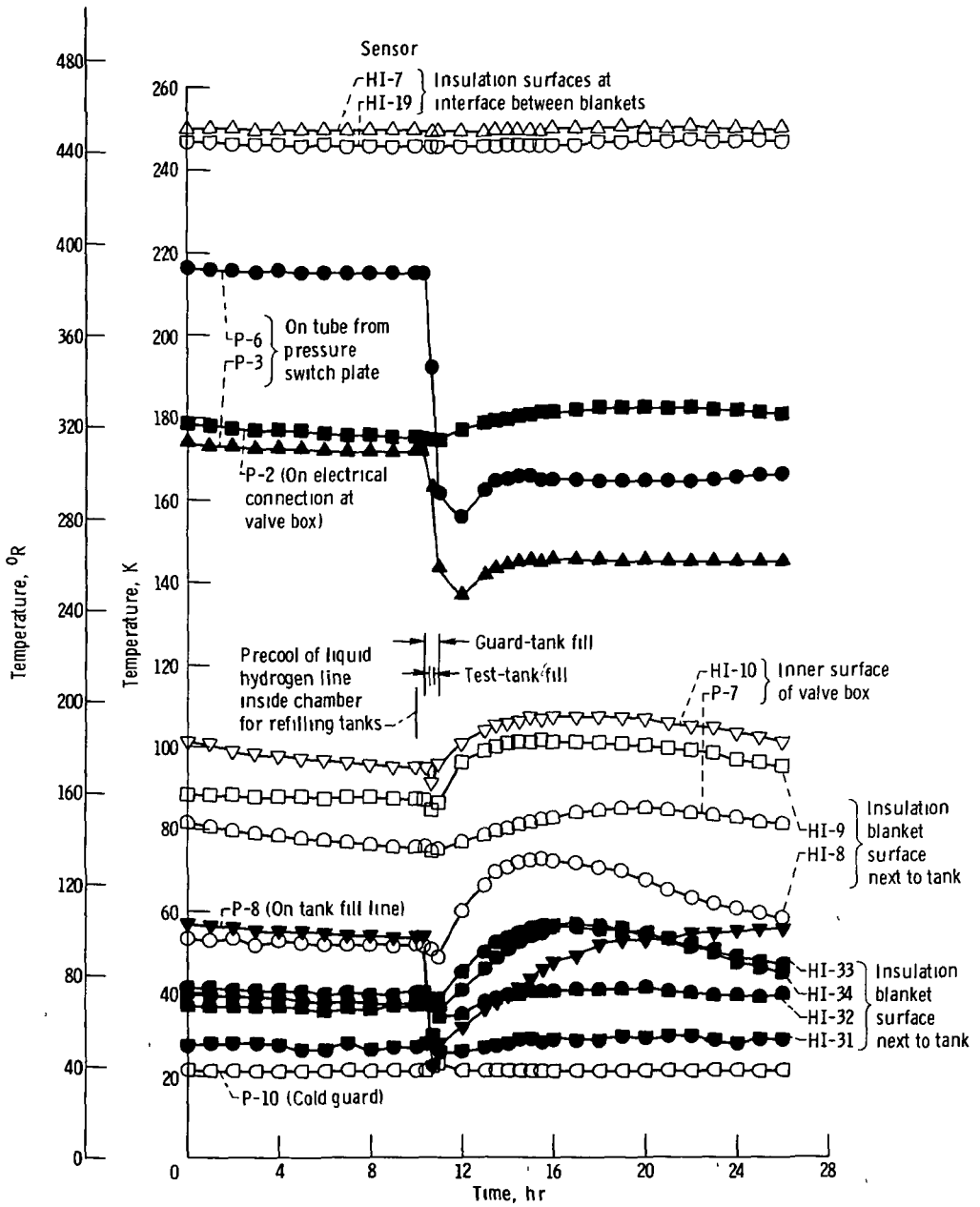

Figure 37 - Response of insulation and line temperatures during refilling of cold guard and test tanks - test NE-7

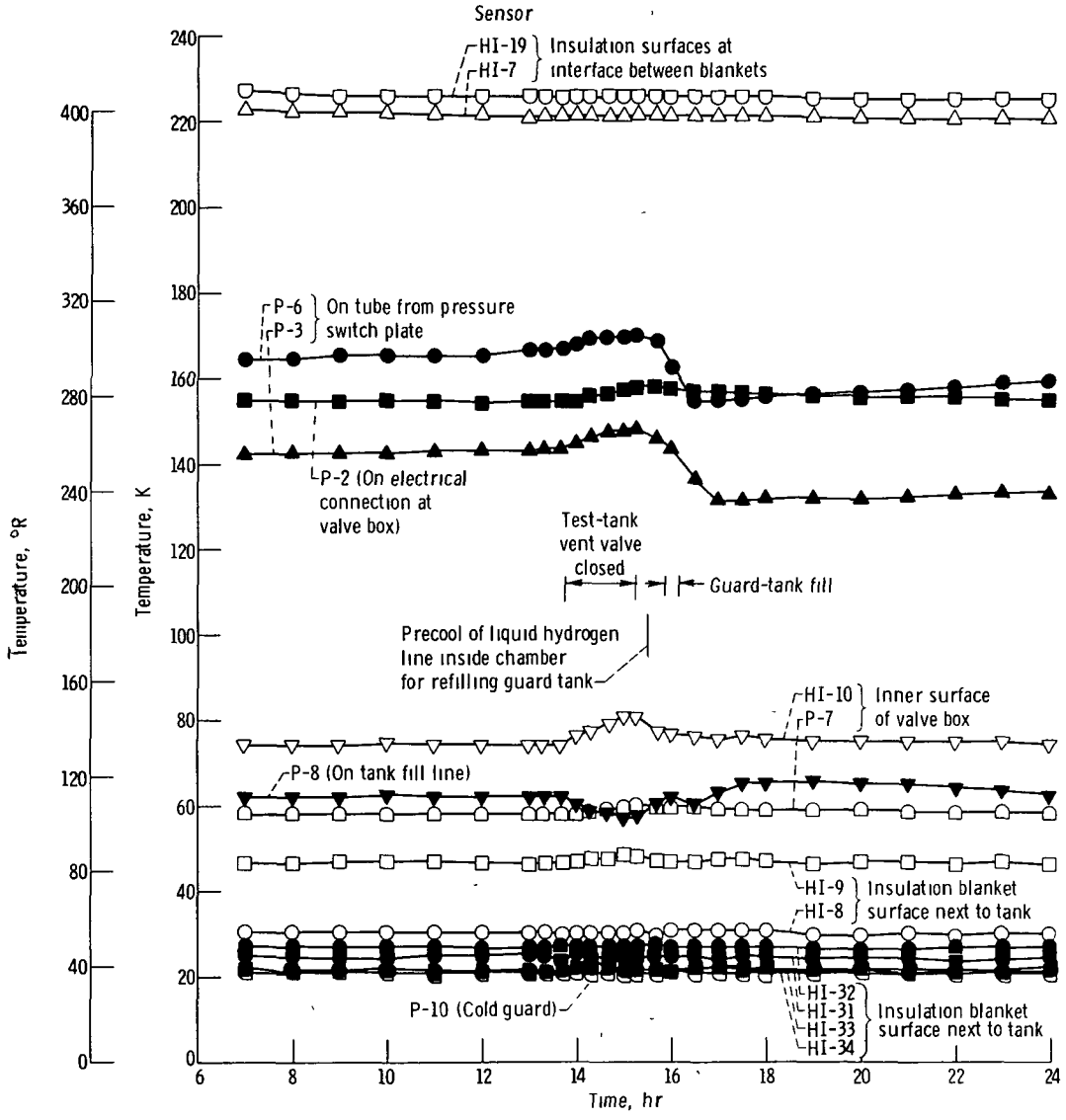

Figure 38 - Response of insulation and line temperatures during vent valve closure and refilling of cold guard tank - test NE-9

"The aeronautical and space activities of the United States shall be conducted so as to contribute . . to the expansion of human knowledge of phenomena in the atmosphere and space The Administration shall provide for the widest practicable and appropriate dissemination of information concerning its activities and the results thereof"

—NATIONAL AERONAUTICS AND SPACE ACT OF 1958

NASA SCIENTIFIC AND TECHNICAL PUBLICATIONS

TECHNICAL REPORTS Scientific and technical information considered important, complete, and a lasting contribution to existing knowledge.

TECHNICAL NOTES Information less broad in scope but nevertheless of importance as a contribution to existing knowledge

TECHNICAL MEMORANDUMS Information receiving limited distribution because of preliminary data, security classification, or other reasons Also includes conference proceedings with either limited or unlimited distribution.

CONTRACTOR REPORTS Scientific and technical information generated under a NASA contract or grant and considered an important contribution to existing knowledge

TECHNICAL TRANSLATIONS Information published in a foreign language considered to merit NASA distribution in English

SPECIAL PUBLICATIONS Information derived from or of value to NASA activities Publications include final reports of major projects, monographs, data compilations, handbooks, sourcebooks, and special bibliographies.

TECHNOLOGY UTILIZATION PUBLICATIONS Information on technology used by NASA that may be of particular interest in commercial and other non-aerospace applications Publications include Tech Briefs, Technology Utilization Reports and Technology Surveys.

Details on the availability of these publications may be obtained from:

SCIENTIFIC AND TECHNICAL INFORMATION OFFICE

NATIONAL AERONAUTICS AND SPACE ADMINISTRATION

Washington, D.C. 20546